diameter of all nodules was 14 mm (range: 5–25 mm), with a mean diameter of 17 mm (range: 8–25 mm) for MNs and 10 mm (range: 5–17 mm) for BNs. These nodules were classified as 35 malignant lesions (primary lung carcinoma in 33 patients [adenocarcinoma in 31 patients and squamous cell carcinoma in 2 patients] and metastatic pulmonary tumor in 2 patients [breast cancer and colon cancer in 1 patient each]; Table 1) and 27 benign lesions (nonspecific benign lesion in 16 patients, granuloma in 4 patients, hamartoma in 3 patients, organized pneumonia in 1 patient, tuberculoma in 1 patient, pulmonary infarction in 1 patient, and pneumonia in 1 patient; Table 2). The primary lung carcinomas were surgically resected in 29 patients, with the exception of 4 patients with adenocarcinoma. The pathologic stage of the resected tumor was histopathologically graded as stage I in 24 patients, stage II in 1 patient, and stage III in 4 patients. The degree of differentiation of the adenocarcinomas in 27 patients was highly differentiated in 11 patients, moderately differentiated in 14 patients, and poorly differentiated in 2 patients. Metastatic lung tumors were found in these 2 patients based on CT fluoroscopy-guided biopsy. Benign lesions were surgically resected in 4 patients (granuloma, organized pneumonia, tuberculoma, and pulmonary infarction) and identified based on CT fluoroscopy-guided biopsy in 6 patients (hamartoma in 3 patients and granuloma in 3 patients). The nodule disappeared in 1 patient with pneumonia, whereas the remaining 16 patients were diagnosed with a nonspecific benign lesion based on the shape of the lesion and changes in

TABLE 1. Characteristics and Quantitative Characterization of MNS

Patient No.	Age (y)	Sex	Diameter (mm)	Lobe	Linear Discriminant Function			Diagnosis
					Non-Enhanced	2 Min*	4 Min*	
1	5	F	18	RU	1.49	4.42	17.42	W/d AD
2	48	F	18	LU	1.64	10.92	16.95	W/d AD
3	77	M	12	LU	2.4	7.14	24.9	AD
4	68	F	22	RL	4.01	15.77	21.8	M/d AD
5	68	M	11	LU	0.85	6.77	8.18	M/d AD
6	54	F	22	LL	1.96	13.29	14.84	Breast matastasis
7	63	M	12	RU	1.41	9.72	14.77	W/d AD
8	63	M	17	RL	2.25	2.65	9.38	M/d AD
9	55	F	18	LU	3.07	12.34	19.49	M/d AD
10	44	M	15	RU	4.65	4.97	11.71	M/d AD
11	61	F	20	RL	3.21	10.01	17.65	W/d AD
12	84	M	19	LU	3.24	11.07	13.36	AD
13	57	M	15	RU	1.88	9.82	21.61	M/d AD
14	71	M	20	LU	1.11	9.83	13.27	AD
15	61	M	13	RM	1.99	14.51	12.78	Colon matastasis
16	51	F	8	LU	0.93	1.58	9.09	W/d AD
17	51	M	18	LU	3.29	13.02	9.37	P/d AD
18	67	M	15	RU	0.89	12.23	14.58	M/d AD
19	62	F	11	RU	0.87	2.39	22.01	W/d AD
20	61	F	25	RM	1.58	9.56	8.77	W/d AD
21	49	F	19	RM	3.16	13.22	22.45	M/d AD
22	63	F	14	LU	1.32	11.5	9.56	W/d AD
23	45	M	12	RU	1.25	0.58	5.44	M/d AD
24	52	M	18	LU	3.4	9.82	13.59	M/d AD
25	56	F	13	RU	0.28	8.12	17.16	W/d AD
26	53	M	24	RU	2.77	14.89	22.35	M/d AD
27	65	F	23	LU	4.28	16.62	27.11	M/d AD
28	71	F	10	RU	−2.16	5.13	5.27	W/d AD
29	66	F	19	LU	2.68	6.95	18.72	P/d AD
30	40	F	19	RL	2.56	5.87	17.62	M/d AD
31	77	F	16	RU	−0.48	5.56	1.81	M/d AD
32	66	M	15	LL	2.26	23.14	2.95	AD
33	80	M	11	RL	0.13	2.19	22.44	M/d AD
34	68	F	19	RU	5.01	14.78	20.36	W/d AD
35	58	F	24	RL	3.25	15.25	22.56	M/d AD

*Time after administration of contrast agent.

AD indicates adenocarcinoma; F, female; LLL, left lower lobe; LUL, left upper lobe; M, male; M/d, moderately differentiated; P/d, poorly differentiated; RLL, right lower lobe; RML, right middle lobe; RUL, right upper lobe; SQ, squamous cell carcinoma; W/d, well differentiated.

TABLE 2. Characteristics and Quantitative Characterization of BNS

Patient No.	Age (y)	Sex	Diameter (mm)	Lobe	Linear Discriminant Function			Diagnosis
					Non-Enhanced	2 Min*	4 Min*	
36	51	F	9	RU	−4.24	−12.77	−11.83	Nonspecific†
37	57	F	10	LU	−1.03	−14.41	−10.29	Hamartoma
38	56	F	15	LU	1.82	−7.56	−3.29	Granuloma
39	65	F	8	RM	−4.68	−11.38	−10.45	Nonspecific†
40	52	F	10	LU	−0.64	−6.93	−17.34	Nonspecific†
41	72	F	10	LL	1.25	3.56	−10.7	Granuloma
42	61	M	7	RL	−3.71	−9.15	−16.22	Nonspecific†
43	70	M	9	RU	−1.21	−7.04	−18.99	Organizing/pneumonia
44	68	F	17	LU	0.97	−3.98	−17.41	Pulmonary/infarction
45	47	F	5	RU	−5.3	−18.14	−32.32	Granuloma
46	56	F	12	RU	−0.85	−18.61	−10.88	Tuberculoma
47	59	F	9	LL	−4.81	−9.74	−19.01	Nonspecific†
48	62	F	12	RM	2.14	−5.63	−4.22	Nonspecific†
49	61	F	6	RM	−5.3	−9.09	−23.16	Nonspecific†
50	60	F	8	RU	−3.53	−18.94	−42.75	Nonspecific†
51	68	F	12	RU	0.54	−19.49	−15.17	Nonspecific†
52	67	M	6	RU	−5.3	−12.58	−21.51	Nonspecific†
53	68	M	8	LL	−4.28	−5.13	−27.26	Nonspecific†
54	64	M	8	RM	−3.82	−7.12	−19.13	Hamartoma
55	70	F	15	RM	2.57	−12.02	−38.67	Nonspecific†
56	60	M	15	RL	−0.49	−5.23	−11.81	Nonspecific†
57	53	F	15	RU	1.2	0.83	−7.36	Granuloma
58	73	M	10	LL	−0.08	0.89	−4.16	Pneumonia
59	72	M	17	LL	−3.24	−9.6	−9.89	Nonspecific†
60	58	M	7	RU	−4.94	−14.21	−10.37	Hamartoma
61	45	M	7	LL	−5.3	−11.81	−6.44	Nonspecific†
62	43	F	8	RL	−3.47	−9.39	−14.15	Nonspecific†

*Time after administration of contrast agent.
†The clinical diagnosis of a nonspecific benign lesion was based on no nodule growth for 2 years or longer.
F, female; LLL, left lower lobe; LUL, left upper lobe; M, male; M/d, moderately differentiated; P/d, poorly differentiated; RLL, right lower lobe; RML, right middle lobe; RUL, right upper lobe; W/d, well differentiated.

size during a follow-up observation period of 2 years or more.[4,17]

This study was approved by the ethical committee of our institution. Written informed consent was obtained from the patients.

RESULTS

Receiver operating characteristic curves were used to evaluate the effectiveness of the diagnostic method using the histogram characteristic values of the attenuation, curvedness value, and shape index to differentiate between BNs and MNs. Evaluation was performed for each parameter as well as for values obtained at different time points: before enhancement and 2 and 4 minutes after enhancement.

The areas under the ROC curve for the attenuation before, 2 minutes after, and 4 minutes after contrast enhancement were 0.58 ± 0.07, 0.69 ± 0.07, and 0.57 ± 0.08, respectively (Fig. 4A); those for the curvedness value were 0.78 ± 0.06, 0.83 ± 0.05, and 0.76 ± 0.06, respectively (see Fig. 4B); and those for the shape index were 0.90 ± 0.04, 0.89 ± 0.05, and 0.90 ± 0.04, respectively (see Fig. 4C). The results for evaluation of all 3 parameters combined were 0.91 ± 0.04, 0.99 ± 0.01, and 1.00, respectively (see Fig. 4D).

Evaluation based on all 3 parameters combined gave the best results. The changes in the linear discriminant function scores over time were analyzed for these combined parameters.

The mean scores before enhancement were −2.06 ± 2.70 (range: −5.3–2.57) for BNs and 2.09 ± 1.50 (range: −2.16–5.01) for MNs. Those at 2 and 4 minutes after enhancement were 9.59 ± 5.04 (range: 0.58–23.1) and 15.1 ± 6.50 (range: 1.81–27.1), respectively, for MNs (see Table 1) and −9.43 ± 5.94 (range: −19.5–3.56) and −16.1 ± 9.94 (range: −42.8 to −3.29), respectively, for BNs (see Table 2). The linear discriminant function scores for MNs were significantly higher than those for BNs at all 3 time points: before enhancement ($P < 0.001$), 2 minutes after enhancement ($P < 0.001$), and 4 minutes after enhancement ($P < 0.001$).

When a linear discriminant function score of 0 or higher was considered to indicate malignancy, there were 2 false-negative (FN) findings (cases 28 and 31) and 7 false-positive (FP) findings (cases 38, 41, 44, 48, 51, 55, and 57) before

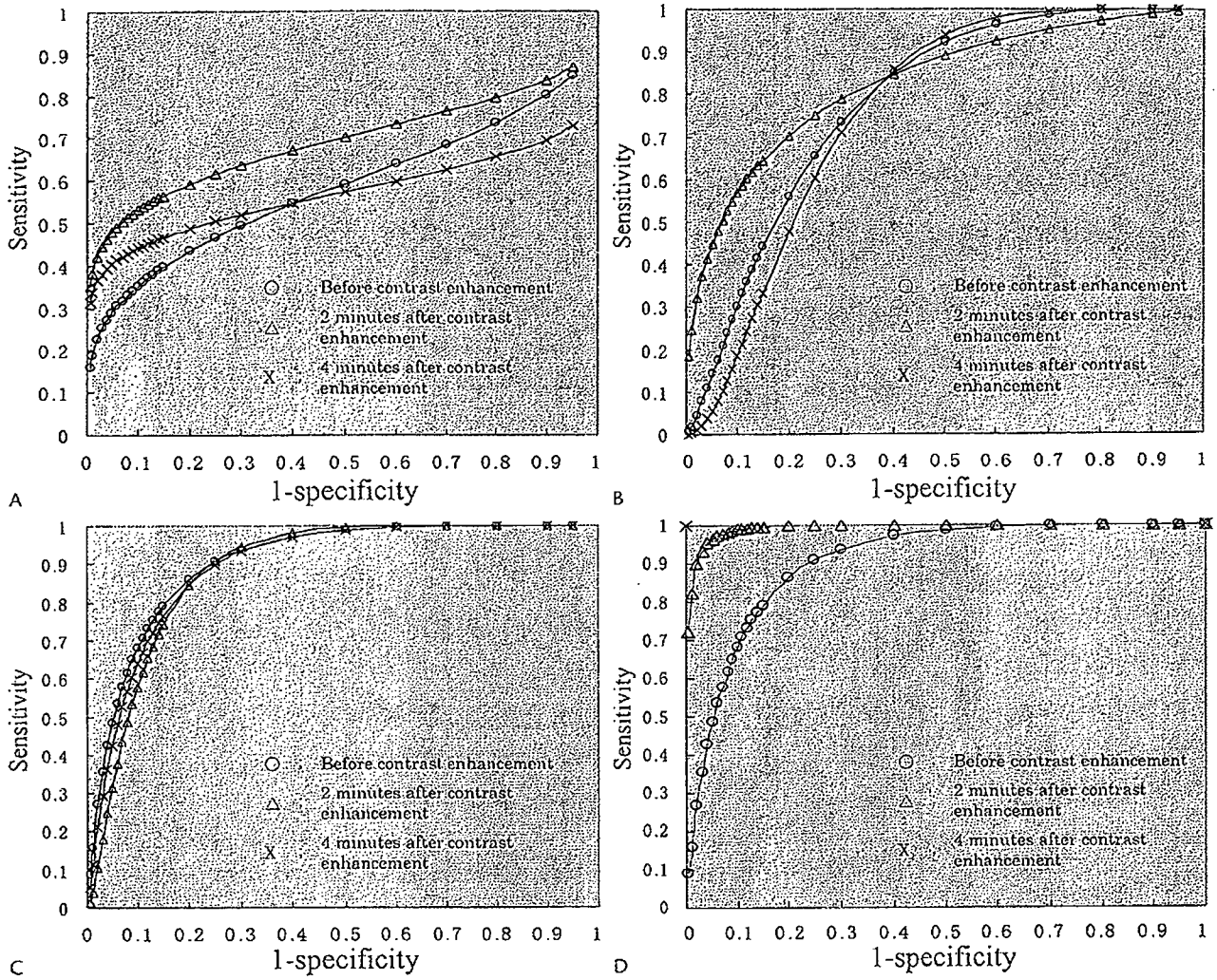

FIGURE 4. Receiver operating characteristic curves for each parameter used to differentiate between malignant and benign nodules. The open circles (O) are before contrast enhancement, and the open triangles (Δ) and crosses (x) are 2 and 4 minutes after contrast enhancement, respectively. A, Areas under the open circle (O), open triangle (Δ), and cross (x) curves for attenuation are 0.58 ± 0.07, 0.69 ± 0.07, and 0.57 ± 0.08, respectively. B, Areas under the open circle (O), open triangle (Δ), and cross (x) curves for curvedness value are 0.78 ± 0.06, 0.83 ± 0.05, and 0.76 ± 0.06, respectively. C, Areas under the open circle (O), open triangle (Δ), and cross (x) curves for shape index are 0.90 ± 0.04, 0.89 ± 0.05, and 0.90 ± 0.04, respectively. D, Areas under the open circle (O), open triangle (Δ), and cross (x) curves for the combination of all 3 parameters (attenuation, shape index, and curvedness value) are 0.91 ± 0.04, 0.99 ± 0.01, and 1.00, respectively.

enhancement, 0 FN findings and 3 FP findings (cases 41, 57, and 58) 2 minutes after enhancement, and 0 FN findings and 0 FP findings 4 minutes after enhancement. Sensitivity values were 94%, 100%, and 100%; specificity values were 74%, 89%, and 100%; and accuracy values were 85%, 92%, and 100%, respectively. Positive predictive values were 83%, 92%, and 100%, and negative predictive values were 91%, 100%, 100%, respectively.

DISCUSSION

The usefulness of diagnostic imaging, focusing mainly on CT, for the evaluation of SPNs has been reported by researchers at a number of medical institutions.[1–4] Several of them have also attempted to differentiate between benign and malignant lesions by using contrast medium and evaluating attenuation within nodules over time.[5–8] These studies were based on attenuation and contrast enhancement patterns obtained for only a few slices in which the nodule was demonstrated, however.

In the present study, the entire nodule was scanned using CE dynamic HCT, and changes in the density and characteristic values (attenuation, shape index, and curvedness value) within the nodule were calculated for 3D quantification with a computer to discriminate between benign and malignant lesions. Contrast-enhanced dynamic HCT in combination with

the computer-aided diagnosis may thus improve the differential diagnosis of BNs and MNs.

With regard to the evaluation and interpretation of the CT data on the lesion, conventional studies have focused only on the 2-dimensional assessment of attenuation and the enhancement patterns in a few slices. The results of these studies were simple and practical, identifying the factors effective for the differential diagnosis to be an observed contrast effect of 20 Hounsfield units (HU) or greater[5,6] or 15 HU or greater,[8] enhancement of the entire lesion,[5] and a high CT value ratio between the nodule and arteries.[7] One problem was that the attenuation was strongly affected by the slice selected or the position of the ROI in the lesion, which was set manually. In the present study, this problem was avoided by automatically extracting the lesion as 3D volume data.[9,12] In addition, the nodule was evaluated by calculating the characteristic values within the nodule using a computer and measuring the density using 3 parameters (attenuation, shape index, and curvedness value).[10] The results showed that evaluation based on the combination of all 3 parameters provided the best results. Using this analysis method, each pixel within a tumor is expressed locally using the attenuation and the shape index and curvedness obtained from the 3D curvature, and the entire lesion is then characterized as benign or malignant using the histogram characteristic values. When these 3 histogram characteristic values were compared with each another, the shape histogram characteristic value was found to be superior to the other 2 values. The combination of these 3 characteristic values provided even better results. It is thought that a more detailed characteristic value for the internal structure of a tumor can be obtained by expressing the internal structure as a combination of attenuation and 3D curvatures.

When a linear discriminant function score not less than 0 at 2 and 4 minutes after enhancement was considered to indicate malignancy, the results showed 0 FN findings and 3 FP findings at 2 minutes after enhancement and no FN or FP findings at 4 minutes. When a linear discriminant function score of 0 or higher was considered to indicate malignancy, benign and malignant lesions were distinguished in all the patients using the data obtained 4 minutes after enhancement. It was considered that the values at 2 minutes were affected by the degree of minute blood vessel density within the nodule and that the values at 4 minutes were affected by the rate of contrast medium flowing into the papillary vessels and interstitial tissues or by the volume of the interstitial tissues.[18] In summary, compared with the techniques used in previous studies, the method described in the present study permits lesions to be extracted with fewer manual operations and higher reproducibility and is based on 3D analysis using 3 parameters (attenuation, shape index, and curvedness value).

The limitations of the present study are as follows. Although the objective of this study was to evaluate the entire nodule, it was difficult to visualize the entire nodule over time, even when an HCT scanner was used. As a result, lesions could not be assessed in 10 patients. It is expected that this problem can be overcome by the introduction of multislice HCT scanners in the near future. In this study, the score was assessed at each time point (before contrast enhancement and 2 and 4 minutes after contrast enhancement). In a strict sense, these scores do not represent the changes in the density of the lesion over time. In the assessment of changes over time, it is important to acquire CT images in exactly the same slice at each time point. The changes over time can then be obtained by performing subtraction between the images before and after contrast enhancement. In practice, however, it is difficult to acquire exactly the same slice at each time point because of the patient's respiratory motion. We are currently working to develop a new algorithm to overcome this problem. When this algorithm is complete, we plan to assess the changes in contrast medium density in lesions over time using subtraction.

In the future, CT-based lung cancer screening is expected to become more widely accepted, resulting in the detection of a larger number of SPNs.[19,20] Therefore, it is likely to become increasingly important to determine whether these lesions are benign or malignant based on evaluation of the images obtained.

Contrast-enhanced dynamic HCT was used for the computer-aided diagnosis of SPNs in the present study. The data obtained using this imaging technique permit the internal structure of lesions to be quantified in a 3D manner and evaluated over time. The results showed that this method is effective for differentiating between BNs and MNs. In the future, further prospective studies should be conducted based on the results reported here and standards for the evaluation of lesions using computer-aided analysis should be established.

REFERENCES

1. Mori K, Saitou Y, Tominaga K, et al. Small nodular lesions in the lung periphery: new approach to diagnosis with CT. *Radiology.* 1990;177: 843–849.
2. Kuriyama K, Tateishi R, Doi O, et al. CT-pathologic correlation in small peripheral lung cancers. *AJR Am J Roentgenol.* 1987;149:1139–1143.
3. Zwirewich CV, Vedal S, Miller RR, et al. Solitary pulmonary nodule; high-resolution CT and radiologic pathologic correlation. *Radiology.* 1991;179:469–476.
4. Siegelman SS, Khouri NF, Leo FR, et al. Solitary pulmonary nodules: CT assessment. *Radiology.* 1986;160:307–312.
5. Yamashita K, Matsunobe S, Tsuda T, et al. Solitary pulmonary nodule: preliminary study of evaluation with incremental dynamic CT. *Radiology.* 1995;194:399–405.
6. Swensen SJ, Brown LR, Colby TV, et al. Lung nodule enhancement at CT; prospective findings. *Radiology.* 1996;201:447–455.
7. Zhang M, Kono M. Solitary pulmonary nodules: evaluation of blood flow patterns with dynamic CT. *Radiology.* 1997;205:471–478.
8. Swensen SJ, Viggiano RW, Midthun DE, et al. Lung nodule enhancement at CT: multicenter study. *Radiology.* 2000;214:73–80.
9. Kawata Y, Niki N, Ohmatsu H, et al. Quantitative surface characterization of pulmonary nodules based on thin-section CT images. *IEEE Trans Nucl Sci.* 1998;45:2132–2138.
10. Kawata Y, Niki N, Mori K, et al. Curvature based analysis of internal structure of pulmonary nodules using thin-section CT images. *Proc IEEE Int Conf Image Processing.* 1998;3:851–855.
11. Armato SG, Li F, Giger ML, et al. Lung cancer: performance of automated lung nodule detection applied to cancers missed in a CT screening program. *Radiology.* 2002;225:685–692.
12. Caselles V, Kimmel R, Sapiro G, et al. Minimal surfaces based object segmentation. *IEEE Trans Pattern Anal Mach Intell.* 1997;19:394–398.
13. Koenderink JJ, van Doorn AJ. Surface shape and curvature scales. *Image Vis Comput.* 1992;10:557–565.

14. Dorai C, Jain AK. COSMOS-A representation scheme for 3D free-form objects. *IEEE Trans Pattern Anal Mach Intell.* 1997;19:1115–1130.
15. Duda RO, Hart PE. Pattern classification and scene analysis. In: Rosen CA, ed. *Linear Discriminant Functions.* New York: John Wiley & Sons; 1973:130–188.
16. Jain AK, Duin RPW, Mao J. Statistical pattern recognition: a review. *IEEE Trans Pattern Anal Mach Intell.* 2000;22:4–37.
17. Yankelevitz DF, Henschke CI. Does 2-year stability imply that pulmonary nodules are benign? *AJR Am J Roentgenol.* 1997;168:325–328.
18. Newhouse JH, Murphy RX. Tissue distribution of soluble contrast: effect of dose variation and changes with time. *AJR Am J Roentgenol.* 1981;136: 463–467.
19. Kaneko M, Eguchi K, Ohmatsu H, et al. Peripheral lung cancer: screening and detection with low-dose spiral CT versus radiography. *Radiology.* 1996;201:798–802.
20. Mori K, Tominaga K, Moriyama N, et al. Utility of low-dose helical CT as a second step after plain chest radiography for mass screening for lung cancer. *J Thorac Imaging.* 1997;12:173–180.

EGFR Mutation Status in Japanese Lung Cancer Patients: Genotyping Analysis Using LightCycler

Hidefumi Sasaki,[1,2] Katsuhiko Endo,[1] Akimitsu Konishi,[1] Minoru Takada,[3] Masaaki Kawahara,[3] Keiji Iuchi,[2] Akihide Matsumura,[2] Meinoshin Okumura,[2] Hisaichi Tanaka,[2] Tomoya Kawaguchi,[3] Toshiki Shimizu,[3] Hiroshi Takeuchi,[3] Motoki Yano,[1] Ichiro Fukai,[1] and Yoshitaka Fujii [1]

Abstract

Purpose: Recently, somatic mutations of the epidermal growth factor receptor (*EGFR*) gene were found in ~25% of Japanese lung cancer patients. These *EGFR* mutations are reported to be correlated with clinical response to gefitinib therapy. However, DNA sequencing using the PCR methods described to date is time-consuming and requires significant quantities of DNA; thus, this existing approach is not suitable for a routine pretherapeutic screening program.

Experimental Design: We have genotyped *EGFR* mutation status in Japanese lung cancer patients, including 102 surgically treated lung cancer cases from Nagoya City University Hospital and 16 gefitinib-treated lung cancer cases from Kinki-chuo Chest Medical Center. The presence or absence of three common *EGFR* mutations were analyzed by real-time quantitative PCR with mutation-specific sensor and anchor probes.

Results: In exon 21, *EGFR* mutations (CTG → CGG; L858R) were found from 8 of 102 patients from Nagoya and 1 of 16 from Kinki. We also detected the deletion mutations in exon 19 from 7 of 102 patients from Nagoya (all were deletion type 1a) and 4 of 16 patients from Kinki (one was type 1a and three were type 1b). In exon 18, one example of G719S mutation was found from both Nagoya and Kinki. The L858R mutation was significantly correlated with gender (women versus men, $P < 0.0001$), Brinkman index (600 ≦ versus 600>, $P = 0.001$), pathologic subtypes (adenocarcinoma versus nonadenocarcinoma, $P = 0.007$), and differentiation status of the lung cancers (well versus moderately or poorly, $P = 0.0439$), whereas the deletion mutants were not. *EGFR* gene status, including the type of *EGFR* somatic mutation, was correlated with sensitivity to gefitinib therapy. For example, some of our gefitinib-responsive patients had L858R or deletion type 1a mutations. On the other hand, one of our gefitinib-resistant patients had a G719S mutation.

Conclusions: Using the LightCycler PCR assay, the *EGFR* L858R mutation status might correlate with gender, pathologic subtypes, and gefitinib sensitivity of lung cancers. However, further genotyping studies are needed to confirm the mechanisms of *EGFR* mutations for the sensitivity or resistance of gefitinib therapy for the lung cancer.

Lung cancer is a major cause of death from malignant diseases because of its high incidence, malignant behavior, and lack of major advancements in treatment strategy (1). Lung cancer was the leading indication for respiratory surgery (42.2%) in 1998 in Japan (2). More than 15,000 patients underwent surgical operation at Japanese institutions in 1998 (2). The clinical behavior of the lung cancer is largely associated with its stage. The cure of the disease by surgery is only achieved in cases representing an early stage of lung cancer (3).

The epidermal growth factor receptor (*EGFR*) tyrosine kinase inhibitor, gefitinib, has been approved in Japan for the treatment of non-small cell lung cancer from 2002. Although *EGFR* is more abundantly expressed in lung carcinoma (4, 5), *EGFR* expression, as detected by immunohistochemistry, did not reveal any obvious relationship with response to gefitinib (6). Clinical trial have revealed significant variability in the response to gefitinib, with higher response in Japanese patients than in predominantly European-derived population (27.5% versus 10.4%; ref. 7). The partial clinical responses to gefitinib have been observed most frequently in women, in nonsmokers, and in patients with adenocarcinoma (8–10). More recently, we have collaborated with Dana-Farber Cancer Institute and found that novel *EGFR* mutations status at ATP binding pockets in Japanese non-small cell lung cancer patients were correlated with the clinicopathologic features related to good response to gefitinib (11). Actually, *EGFR* mutations in lung cancer have been correlated with clinical response to gefitinib therapy *in vivo* and *in vitro* (11–13).

Authors' Affiliations: [1]Department of Surgery II, Nagoya City University Medical School, Nagoya, Japan and Departments of [2]Surgery and [3]Internal Medicine, National Hospital Organization, Kinki-chuo Chest Medical Center, Sakai, Japan
Received 9/16/04; revised 12/4/04; accepted 1/19/05.

Grant support: Grant-in-aid for Cancer Research (16-1) from the Ministry of Health, Labour and Welfare, and AstraZeneca research grant 2004.

The costs of publication of this article were defrayed in part by the payment of page charges. This article must therefore be hereby marked *advertisement* in accordance with 18 U.S.C. Section 1734 solely to indicate this fact.

Requests for reprints: Hidefumi Sasaki, Department of Surgery II, Nagoya City University Medical School, 1 Kawasumi, Mizuho-cho, Mizuho-ku, Nagoya, Aichi 467-8601, Japan. Phone: 81-52-853-8231; Fax: 81-52-853-6440; E-mail: hisasaki@med.nagoya-cu.ac.jp.

The standard for experimental detection of mutations is direct sequencing of DNA samples from the tissues. For known mutations, real-time polymerase chain detection followed by melting curve analysis, using hybridization probes, is highly sensitive, rapid, and an efficient alternative approach to mutation detection (14–16).

To determine the *EGFR* mutation status in Japanese lung carcinoma for screening and diagnostic purposes, we wanted to develop a faster and easy method to detect *EGFR* mutations. In this report, we investigated *EGFR* mutation status by the real-time reverse transcription-PCR assay using LightCycler (17) mutation-specific sensor and anchor probes. With this method, 32 samples were genotyped within 1 hour without the need of any post-PCR sample manipulation. The findings were compared with the clinicopathologic features of lung cancer.

Materials and Methods

Patients. The study group included 102 lung cancer patients who had undergone surgery (but did not receive gefitinib) at the Department of Surgery II, Nagoya City University Medical School, between 1997 and 2000. The study group also included 16 lung cancer patients who had undergone surgery at the Department of Surgery, National Hospital Organization, Kinki-chuo Chest Medical Center, and were subsequently treated with gefitinib. These 16 samples were sequenced by ABI prism 3100 analyzer (Applied Biosystems Japan, Ltd., Tokyo, Japan; data not shown) and analyzed by ABI prism Seq Scape version 2.1.1. The lung tumors were classified according to the general rule for clinical and pathologic record of lung cancer in Japan (18). All tumor samples were immediately frozen and stored at −80°C until assayed.

The clinical and pathologic characteristics of the 102 lung cancer patients are as follows: 52 cases at stage I, 16 at stage II, and 34 at stage III to IV. The mean age was 65.5 years (range, 42-85). Among the 102 lung cancer patients, 49 (48%) were diagnosed as having adenocarcinoma, 32 (31.4%) squamous cell carcinoma, 9 (8.8%) adenosquamous cell carcinoma, and 7 (6.9%) small cell carcinoma.

PCR assays for EGFR. The genomic DNA was extracted from lung cancer tissues and matched normal lymphocytes from the peripheral blood using the Wizard SV Genomic DNA purification system (Promega Corporation, Madison, WI). Initially, 58 DNA samples were also extracted from lung cancer tissues from Nagoya City University and sequenced as reported in our previous paper (11). These sets of DNA were used as a positive and negative control for genotyping. DNA concentration was determined by spectrophotometry and adjusted to a concentration of 50 ng/mL. We then used 1 μL of each DNA for LightCycler analyses. To ensure the fidelity of DNA extraction, all samples were subjected to PCR amplification with oligonucleotide primers specific for exon 18 of the *EGFR* gene and then digested by *Sac*I enzyme. The primer sequences for *EGFR* gene in exon 18 were as follows: the forward primer, 5-TCCAAATGAGCTGGCAAGTG-3, and the reverse primer, 5-TCCCAAACACTCAGTGAAACAAA-3 (397 bp). The cycling conditions were as follows: initial denaturation at 95°C for 15 minutes followed by 35 cycles at 95°C for 20 seconds, 57°C for 20 seconds, 72°C for 30 seconds, and one cycle of 72°C for 3 minutes. The products were purified by Qiagen PCR purification kit (Qiagen, Valencia, CA) and then digested with restriction enzyme at 37°C for 2 hours. The genotyping PCR reactions were done using LightCycler DNA Master Hybridization probes kit (Roche Molecular Biochemicals, Mannheim, Germany) in a 20 μL reaction volume. The primer sequences for *EGFR* gene in exon 18 were as follows: the forward primer, 5-TCCAATGAGCTGGCAAGTG-3, and the reverse primer, 5-TCCCAAACACTCAGTGAAACAAA-3 (397 bp). For the exon 18 genotyping, sensor (LC Red 640-GCACCGGAGCCCAGCA) and anchor (GCCAGGGACCTTATACACGTGCCGAA-Fluorescein) probes were used. The cycling conditions were as follows: initial denaturation at 95°C for 10 minutes, followed by 45 cycles at 95°C for 10 seconds, 60°C for 10 seconds, and 72°C for 16 seconds The primer sequences for *EGFR* gene in exon 19 were as follows: the forward primer, 5-CGTCTTCCTTCTCTCTCTGTC-3, and the reverse primer, 5-GACATGAGAAAAGGTGGGC-3 (175 bp). For the exon 19 genotyping, sensor (GCTATCAAAACATCTCC-Fluorescein) and anchor (LC Red 640-AAAGCCAACAAGGAAATCCTCGATGTGAGTTTCTGCTTTGCTGTGTGGGG) probes were used. The cycling conditions were as follows: initial denaturation at 95°C for 10 minutes followed by 45 cycles at 95°C for 10 seconds, 60°C for 10 seconds, and 72°C for 7 seconds. The primer sequences for *EGFR* gene in exon 21 were as follows: the forward primer, 5-GCTCAGAGCCTGGCATGAA-3, and the reverse primer, 5-CATCCTCCCCTGCATGTGT-3 (349 bp). The cycling conditions were as follows: initial denaturation at 95°C for 10 minutes, followed by 45 cycles at 95°C for 10 seconds, 57°C for 10 seconds, and 72°C for 14 seconds. For the exon 21 genotyping, sensor (Fluorescein-AGTTTGGCCCGCCCA) and anchor (LC Red 640-CCTCCTTCTGCATGGTATTCTTTCTCTTCCGCACCCAG) probes were used.

Statistical methods. Statistical analyses were done using the Mann-Whitney *U* test for unpaired samples and Wilcoxon's singed rank test for paired samples. Linear relationships between variables were determined by simple linear regression. Correlation coefficients were determined by rank correlation using Spearman's test and χ^2 test. The overall survival of lung cancer patients was examined by the Kaplan-Meier methods and differences were examined by the log-rank test, Breslow-Gehan-Wilcoxon test, and Cox proportional hazard regression model. All analyses were done using the StatView software package (Abacus Concepts, Inc., Berkeley, CA) and results were considered significant when $P < 0.05$.

Results

Fidelity of allele-specific PCR confirmed by conventional PCR assay in lung cancer tissues. Using the exon 18 primer sets, a PCR product of 397 bp was obtained. We have analyzed the product using PCR-RFLP method. The wild-type DNA does not have a *Sac*I site within the 397 bp. The PCR products digested with *Sac*I were loaded with 2% agarose gel and wild-type DNA should be visualized as one band. However, if the substitution mutation G719S were present, the PCR products digested by *Sac*I will be visualized as three bands. Using this method, PCR products were visualized from all lung cancer patients studied. In exon 18, a G719S mutation was found from one Nagoya specimen (stage Ia, well-differentiated adenocarcinoma with bronchioloalveolar carcinoma pattern at the edge of tumor, female, nonsmoker patient) and one Kinki specimen (Fig. 1A). These mutants were also analyzed by LightCycler. The anchor probe was matched for wild type. As shown in Fig. 1B for the G719S mutation in exon 18, the homozygous wild-type PCR product showed a single peak at 69°C, whereas the heterozygous products (mutant) showed an additional peak at 59°C. The LightCycler method using the mutation-specific probes confirmed the results with the restriction fragment analysis.

Genotyping of EGFR at exon 19 and exon 21 in lung cancer tissues. For exon 21 genotyping, the anchor probe was matched for L858R mutation. As shown in Fig. 2, for the L858R mutation in exon 21, the homozygous wild-type PCR product showed a single peak at 53°C, whereas the heterozygous products (mutant) showed an additional peak at 65°C. From the 102 lung cancer patients, 8 patients had the L858R mutation. One was male and seven were female. Seven were nonsmokers and one was a smoker (Brinkman index was 600). All eight patients had adenocarcinoma, one was moderately differentiated, and

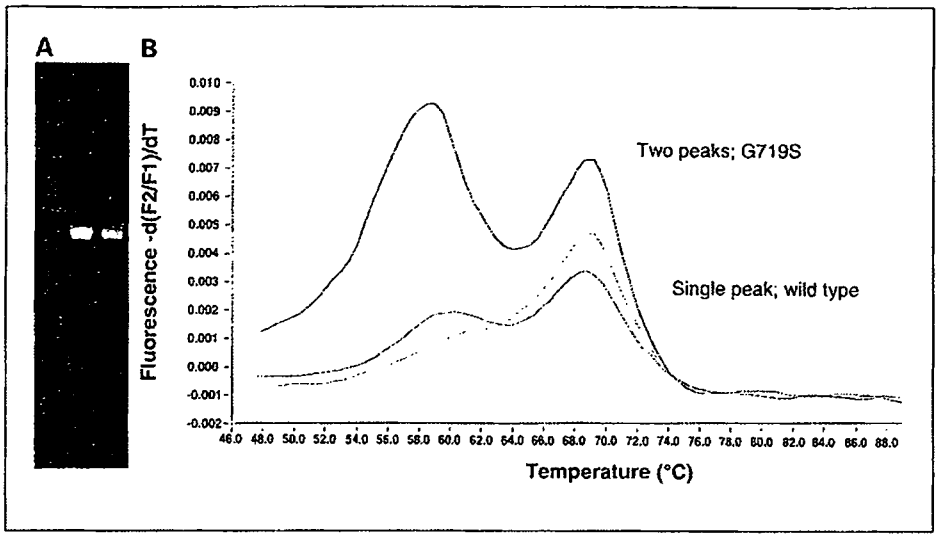

Fig. 1. *A*, analyzed data using PCR-RFLP. Left lane, the wild-type DNA within the 397 bp does not have *Sac*I site. The PCR products restricted with *Sac*I were loaded with 2% agarose gel and was visualized as one band. Right lane, the substitution mutation G719S caused *Sac*I site, and the PCR products restricted by *Sac*I was visualized as three bands. *B*, detection of a G719S mutation in the *EGFR* gene in genomic DNA extracted from lung cancer tissues. The negative derivative of the fluorescence ($-dF / dT$) versus temperature graph shows peaks with different T_m. The wild-type sample showed a single T_m at 69°C. The heterozygous mutant sample showed an additional peak at 59°C.

seven were well differentiated. Five of eight adenocarcinomas showed bronchioloalveolar carcinoma pattern at the edge of tumor. Thus, L858R mutation status was significantly correlated with gender, Brinkman index, pathologic subtypes, and differentiation of lung cancer (Table 1). Eight of eight PCR products from matched peripheral lymphocyte DNA showed a single peak, suggesting that the mutations were somatic. L858R mutation was also found in one nonsmoking female adenocarcinoma patient from Kinki-chuo Chest Medical Center.

For exon 19 genotyping, the anchor probe was matched for deletion type 1a (2,235-2,249 nucleotides deletion; deletion GGAATTAAGAGAAGC) mutation. As shown in Fig. 3, for the deletion 1a mutation in exon 19, the PCR product showed a single peak at 56°C, whereas the deletion 1b products (2,236-2,250 nucleotides deletion; deletion GAATTAAGAGAAGCA) showed a peak at 47°C. From the 102 lung cancer patients, seven patients had the deletion 1a mutation. Four were males and three were females. Three were nonsmokers and four were smokers. Four patients had adenocarcinoma, two had squamous cell carcinoma, and one had adenosquamous cell carcinoma. One of the tumors was moderately differentiated, two were poorly differentiated, and three were well differentiated. One of four adenocarcinomas showed bronchioloalveolar carcinoma pattern at the edge of tumor. Thus, deletion 1a mutation status was not significantly correlated with gender, Brinkman index, pathologic subtypes, and differentiation of lung cancer (Table 2). Five of seven PCR products from matched peripheral lymphocyte DNA were available and showed a single peak, suggesting that these mutations were somatic.

The mutations detected in lung cancer specimens from Kinki-chuo Chest Medical Center are summarized in Table 3. L858R mutation and deletion type 1a were found from partial response patients. On the other hand, G719S mutation was found from a patient with no response to gefitinib (progressive disease). A total of six mutations were found from 16 gefitinib-treated patients (37.5%). Taken together, 22 mutations were found from 117 examined samples in our analysis (18.8%).

The overall survival of 102 lung cancer patients from Nagoya City University, with follow-up through December 30, 2003, was studied in reference to the *EGFR* mutation status. There was no significant difference in the prognosis between the patients with wild-type *EGFR* (n = 86, 22 were dead) and the patients with

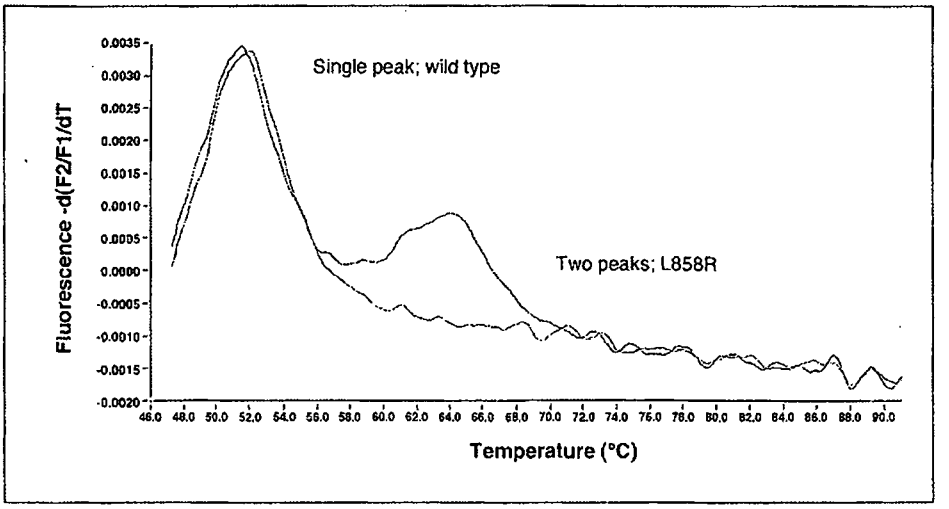

Fig. 2. The L858R mutation in exon 21 of the homozygous wild-type PCR product showed a single peak at 53°C, whereas the heterozygous products (mutant) showed an additional peak at 65°C.

Table 1. Clinicopathologic data of 102 lung cancer patients

Factors	L858R Mutation patients (%)	L858R Wild-type patients (%)	*P*
Mean age (y), 65.5 ± 9.3	8	94	
Stage			
I	7 (87.5)	45 (47.9)	0.0744
II-IV	1 (12.5)	49 (52.1)	
Lymph node metastasis			
N0	7 (87.5)	60 (63.8)	0.3341
N+	1 (12.5)	34 (36.2)	
BI			
≦600	8 (100)	32 (34.0)	0.001
>600	0 (0)	62 (66.0)	
Differentiation			
Well	7 (87.5)	31 (43.1)	0.0439
Moderately or poorly	1 (12.5)	41 (56.9)	
Pathologic subtypes			
Adenocarcinoma	8 (100)	41 (43.6)	0.007
Nonadenocarcinoma	0 (0)	53 (56.4)	
Age			
≦60	2 (25.0)	26 (27.7)	0.9999
>60	6 (75.0)	68 (72.3)	
Gender			
Male	1 (12.5)	80 (85.1)	<0.0001
Female	7 (87.5)	14 (14.9)	

Abbreviations: N+, lymph node metastasis positive; BI, Brinkman index.

mutation in the *EGFR* gene ($n = 16$, two were dead; log-rank test, $P = 0.3608$; Breslow-Gehan-Wilcoxon test, $P = 0.4761$), although the observation period was short.

Discussion

We obtained findings that L858R *EGFR* mutation status was significantly correlated with gender, smoking history, and pathologic subtypes of lung cancers. This was in agreement with the recent reports that *EGFR* gene mutations are common in lung cancers from never smokers (13) and females with adenocarcinoma (11). Our analysis also suggested that the type of *EGFR* mutation might be correlated with the sensitivity of gefitinib therapy for lung cancers.

When the PCR is used for the detection of mutations in very small amounts of DNA, although we would like to start from biopsy samples in the future, it is usually necessary to use "nested PCR." In this case, a DNA fragment is amplified with a first set of primers and part of the product is reamplified with a second set of primers complementary to sequences in the product. Recent developments in fast PCR and real-time detection of products make a more sensitive approach to detection of mutations possible (14–16, 19). We have optimized mutation detection, without nested PCR, using the LightCycler. This instrument measures fluorescence during PCR and can detect the SYBR Green dye when it is intercalated in double-stranded DNA, allowing the detection of double-stranded PCR product formation. The use of labeled probes homologous to the PCR product permits specific identification of PCR products (17). In the LightCycler, two adjacent probes were used, labeled with different fluorescent molecules. When the probes were bound to the single-stranded target, one to five bases apart, the 3′-end label of the 5′ probes came close to the 5′-end label of the 3′ probe, resulting in resonance and strong fluorescence at a specific wavelength. An advantage of this strategy is that hybridization of the probe is not restricted to the temperature range required for Taq polymerase to remove a base (19, 20). Further melting curves can be produced after PCR to assess the dissociation temperature of the probe. Mutations covered by the probe can be detected by a shift in melting temperature. The one-cycle analysis took ~1 hour and could examine 32 samples.

Because so many *EGFR* mutation phenotypes were discovered, it would be of interest to determine whether resistance to *EGFR* inhibition emerges through secondary mutation as is the case in imatinib-treated chronic myelogenous leukemia (21). Our data showed that L858R mutation and deletion type 1a were found in gefitinib-sensitive patients; on the other hand, a G719S mutation was found in a gefitinib-resistant patient. Interestingly, recent data reported that L858R mutant (transfected cell) was inhibited at 10-fold lower concentrations of tyrosine kinase inhibitor; however, the deletion mutant seemed to have similar sensitivities as wild-type *EGFR*

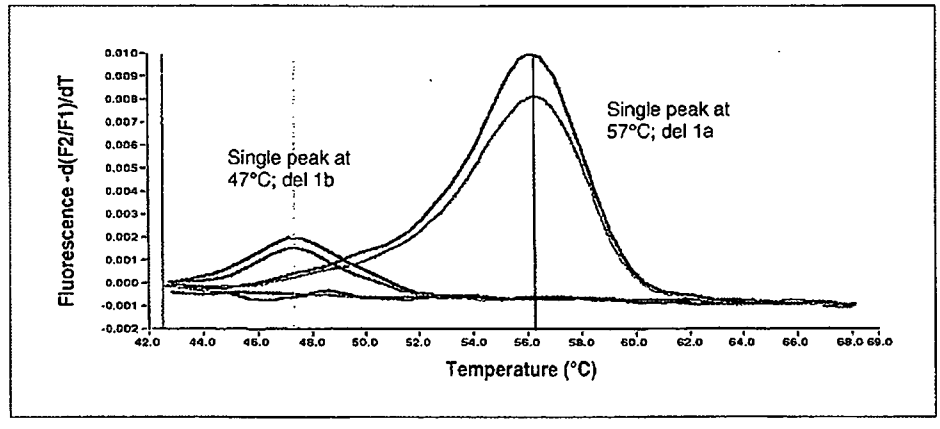

Fig. 3. Detection of the deletion mutations in the *EGFR* gene in genomic DNA extracted from lung cancer. The deletion 1a – type sample showed a single T_m at 56°C. The deletion type 1b sample showed a single peak at 47°C.

Table 2. Clinicopathologic data of 102 lung cancer patients

Factors	Exon 19 deletion: Mutation patients (%)	Exon 19 deletion: Wild-type patients (%)	*P*
Mean age (y), 65.5 ± 9.3	7	95	
Stage			
I	3 (42.9)	49 (51.6)	0.9571
II-IV	4 (57.1)	46 (48.4)	
Lymph node metastasis			
N0	3 (42.9)	64 (67.4)	0.3650
N+	4 (57.1)	31 (32.6)	
BI			
≦600	5 (71.4)	35 (36.8)	0.1592
>600	2 (28.6)	60 (63.2)	
Differentiation			
Well	3 (50.0)	35 (47.3)	0.9999
Moderately or poorly	3 (50.0)	39 (52.7)	
Pathologic subtypes			
Adenocarcinoma	4 (57.1)	45 (47.4)	0.9143
Nonadenocarcinoma	3 (42.9)	50 (52.6)	
Age			
≦60	2 (28.6)	26 (27.4)	0.9999
>60	5 (71.4)	69 (72.6)	
Gender			
Male	4 (57.1)	77 (81.1)	0.3051
Female	3 (42.9)	18 (18.9)	

to drug (13). Thus, mutation phenotypes might be correlated with sensitivity for gefitinib therapy. Substitution mutation L858R is located adjacent to the highly conserved DFG motif in the activation motif. The activation loop was known to be important for autoregulation in many kinases (22). For example, the mutation in the activation loop of insulin receptor tyrosine kinase substantially increases the ability of the unphosphorylated kinase to bind ATP (23). From our data, this mutation pattern (L858R) might be more correlated with the populations, such as women, smoking, and adenocarcinoma.

DNA sequencing using the PCR methods described to date is time-consuming and, therefore, may not be suitable for a regular pretherapeutic screening program. Genechip technology is promising but still in its infancy, and adapting this technology to new polymorphisms is time-consuming and expensive. Real-time PCR, on the other hand, allows for easy adoption of new polymorphisms and possibly provides the best means for pretherapeutic genotyping in a clinical setting at present. We, therefore, developed three different PCRs to detect *EGFR* gene mutations and deletions. The advantages of real-time PCR are extensive. The faster PCR method and elimination of additional steps to analyze PCR products save time and minimize the risks of DNA contamination. Handling is facilitated and potentially toxic reagents, such as ethidium bromide stain, are avoided. We have only found 16 of 101 surgically removed samples from Nagoya City University and 6 of 16 gefitinib-treated samples from Kinki-chuo Chest Medical Center. Other mutations might have existed for these patients, although we have only checked the three most frequent mutations. The difference in the ratio of *EGFR* mutation between Nagoya and Kinki patients might have been caused by selection bias because gefitinib was known to be sensitive for female, nonsmoker, and adenocarcinoma patients. Actually, we have checked seven small cell carcinoma and three large cell carcinoma patients from Nagoya and no mutations were found from these patients.

Using the LightCycler reverse transcription-PCR assay described here, the determination of *EGFR* mutation status may be of clinical importance in predicting the sensitivity or resistance to gefitinib therapy for lung cancer. With this method, 32 samples were genotyped within 1 hour without the need of any post-PCR sample manipulation. Mutation detection using real-time PCR with hybridization probes and

Table 3. Genotyping analyses data for the non–small cell lung cancer patients from Kinki-chuo Chest Medical Center

Age	Gender	Mutation	Exon	Mutation type	Pathology	Smoking history
59	F	+	19	del 1a	Adenocarcinoma	N
69	F	+	18	G719S	Adenocarcinoma	N
76	M	+	19	del 1b	Adenocarcinoma	N
56	M	+	19	del 1b	Adenocarcinoma	F/C
33	M	+	19	del 1b	Adenocarcinoma	F/C
59	F	+	21	L858R	Adenocarcinoma	N
47	M	–			Adenocarcinoma	F/C
65	F	–			Adenocarcinoma	N
51	F	–			Adenocarcinoma	N
66	M	–			Adenocarcinoma	F/C
82	M	–			Adenocarcinoma	F/C
71	F	–			BAC	N
66	F	–			BAC	N
71	F	–			Adenocarcinoma	N

Abbreviations: F, female; M, male; del, deletion; BAC, bronchioloalveolar carcinoma; N, never smoker; F/C, former or current smoker.

melting curve analysis can be used for the sensitive detection of DNA mutations. The fast detection of single base substitutions in small amounts of DNA has great potential in pretreated diagnosis and in oncology.

Acknowledgments

We thank Dr. Matthew Meyerson for critical reading of the manuscript and Naoya Hosono and Atsuko Miyazaki for their excellent technical assistance.

References

1. Ginsberg RJ, Kris K, Armstrong G. Cancer of the lung. 4th ed. In: Principles and Practice of Oncology. Philadelphia: Lippincott 1993;1993. p. 673–82.
2. Yasuda K, Ayabe H, Ide H, Uchida Y; on behalf of the Japanese Association for Thoracic Surgery: Thoracic and cardiovascular surgery in Japan during 1998. Annual report by the Japanese association for thoracic surgery. Jpn J Cardiothorac Surg 1998;48:401–15.
3. Postus PE; on behalf of the Lung Cancer Cooperative Group of the EORTC. The experience of the lung cancer cooperative group of the European Organization for Research and Treatment of Cancer. Chest Suppl 1997;113:28–31S.
4. Rusch V, Baselga J, Cordon-Cardo C, et al. Differential expression of the epidermal growth factor receptor and its ligands in primary non-small cell lung cancers and adjacent benign lung. Cancer Res 1993; 53:2379–85.
5. Sasaki H, Yukiue H, Mizuno K, et al. Elevated serum epidermal growth factor receptor level is correlated with lymph node metastasis in lung cancer. Int J Clin Oncol 2003;8:79–82.
6. Parra HS, Cavina R, Latteri F, et al. Analysis of epidermal growth factor receptor expression as a predictive factor for response to gefitinib ("Iressa," ZD1839) in non-small cell lung cancer. Br J Cancer 2004;91:208–12.
7. Fukuoka M, Yano S, Giaccone G, et al. Multi-institutional randomized phase II trial of gefitinib for previously treated patients with advanced non-small-cell lung cancer. J Clin Oncol 2003;21:2237–49.
8. Janne PA, Gurubhagavatula S, Yeap BY, et al. Outcomes of patient wit advanced non-small cell lung cancer treated with gefitinib (ZD1839, "Iressa") on an expanded access study. Lung Cancer 2004;44:221–30.
9. Kris MG, Natale RB, Herbst RS, et al. Efficacy of gefitinib, an inhibitor of the epidermal growth facto receptor tyrosine kinase, in symptomatic patients with non-small cell lung cancer: a randomized trial. JAMA 2003;290: 2149–58.
10. Miller VA, Kris MG, Shah N, et al. Bronchioloalveolar pathologic subtype and smoking history predict sensitivity to gefitinib in advanced non-small-cell lung cancer. J Clin Oncol 2004;22:1103–9.
11. Paez JG, Janne PA, Lee JC, et al. EGFR mutations in lung cancer: correlation with clinical response to gefitinib therapy. Science 2004;81:61–9.
12. Lynch TJ, Bell DW, Sordella R, et al. Activating mutations in the epidermal growth factor receptor underlying responsiveness of non-small-cell lung cancer to gefitinib. N Engl J Med 2004;53:1192–202.
13. Pao W, Miller V, Zakowski M, et al. EGF receptor gene mutations are common in lung cancers from "never smokers" and are associated with sensitivity of tumors to gefitinib and elrotinib. Proc Natl Acad Sci U S A 2004;101:13306–11.
14. Wittwer CT, Herrmann MG, Moss AA, Rasmussen RP. Continuous fluorescence monitoring of rapid cycle DNA amplification. BioTechniques 1997;22: 130–8.
15. Wittwer CT, Reed GB, Ririe KM. Rapid cycle amplification. In: Mullis KB, Ferre F, Gibbs RA, editors. The polymerase chain reaction. Boston: Birkhauser; 1994. p. 174–81.
16. Pals G, Pindolia K, Worsham MJ. A rapid and sensitive approach to mutation detection using real-time polymerase chain reaction and melting curve analyses, using BRCA1 as an example. Mol Diagn 1999;4:241–6.
17. Wittwer T, Ririe M, Andrew V, David A, Gungry A, Bali J. The LightCycler: a microvolume multisample fluorimeter with rapid temperature control. BioTechniques 1997;22:176–81.
18. Japan Lung Cancer Society. General rule for clinical and pathological record of lung cancer. 5th ed. Tokyo: Japan Lung Cancer Society 1999; p. 1–177.
19. Pals G, Young C, Mao HS, Worsham MJ. Detection of a single base substitution in a single cell using the LightCycler. J Biochem Biophys Methods 2001;47: 121–9.
20. Heid CA, Stevens J, William PM. Real time quantitative PCR. Genome Res 1996;6:986–94.
21. Gorre ME, Mohammed M, Ellwood K, et al. Clinical resistance to STI-571 cancer therapy caused by BCR-ABL gene mutation or amplification. Science 2001; 293:876–80.
22. Huse M, Kuriyan J. The conformational plasticity of protein kinases. Cell 2002;109:275–82.
23. Till JH, Ablooglu AJ, Frankel M, Bishop SM, Kohanski RA, Hubbard SR. Crystallographic and solution studies of an activation loop mutant of the insulin receptor tyrosine kinase: insights into kinase mechanism. J Biol Chem 2001;276:10049–55.

EGFR阻害薬と他の分子標的治療薬との併用療法

大原房子* 高野利実* 大江裕一郎*

はじめに—分子標的治療薬の併用療法の背景—

分子標的治療薬は近年の癌治療において欠かせないものとなってきている．わが国では上皮成長因子レセプター（EGFR）チロシンキナーゼ阻害薬（EGFR-TKI）であるゲフィチニブが，非小細胞肺癌（NSCLC）の治療薬として2002年世界に先駆けて承認された[1]．その後の研究や臨床試験によって，ゲフィチニブはEGFR遺伝子変異のあるNSCLCに劇的な効果をもたらすなど[2][3]，その分子生物学的特性が明らかになりつつある．しかし，EGFR遺伝子変異のないNSCLCでは多くの場合効果が期待できないことや，EGFR遺伝子変異のある場合でも治療中に耐性化するケースが少なくないことなど，新たな問題点も認識されはじめた．EGFR遺伝子変異がゲフィチニブの効果を規定する因子や獲得耐性が生じる機序を解明し，耐性克服への道筋をつけることが今後の課題である．

耐性克服の方法としてまず考えられるのが多剤併用療法であるが，ゲフィチニブと従来の抗癌剤との併用では有望な結果は得られていない．NSCLCのファーストライン化学療法として，ゲフィチニブに既存の抗癌剤を併用した2つの大規模臨床試験がおこなわれたが[4][5]，いずれも生存率の改善は認められなかった．この原因として，適切な患者選択がなされていなかったことのほかに，ゲフィチニブの増殖抑制効果が，結果的には抗癌剤の細胞に対する感受性を弱めてしまった可能性が考えられている[6]．

これらの問題点を解決しうる方法として期待されているのが，EGFR阻害薬と他の分子標的治療薬との併用療法である．現在検討されているおもな組み合わせとして，1）EGFR-TKIと抗EGFR（もしくはHER2）レセプターモノクローナル抗体，2）EGFR阻害薬とEGFR下流シグナル経路（PI-3K—AKT経路，Ras—MAPK経路などAKTやMAPK）（図❶）[7]の阻害薬，3）EGFR阻害薬と細胞内シグナル伝達阻害薬，4）EGFR阻害薬と血管新生阻害薬などがあげられるが，現在臨床応用されているものは1）もしくは4）である（表❶）．1）に相当するものとして，転移性乳癌に対してゲフィチニブと抗HER2モノクローナル抗体であるトラスツズマブを併用する臨床試験[8][9]，腎細胞癌・大腸癌・NSCLCに対してerlotinib（EGFR-TKI）とcetuximab（抗EGFRモノクローナル抗体）を併用する臨床試験などがおこなわれている．また，4）

*OHARA Fusako, TAKANO Toshimi, OHE Yuichiro／国立がんセンター中央病院内科

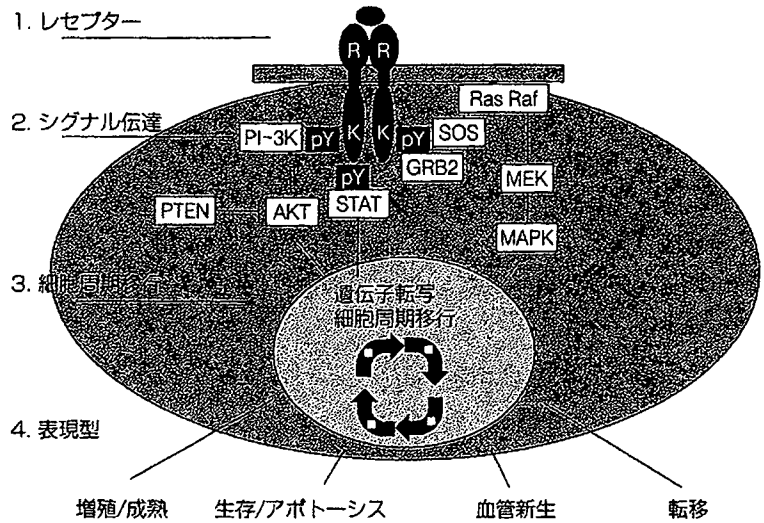

図❶ EGFR シグナル伝達経路
(Baselga J, 2001[7]より引用)

表❶ 分子標的治療薬同士を併用した臨床試験

分子標的治療薬		Phase	対象臓器	NCI Protocol ID/報告者
ゲフィチニブ	トラスツズマブ	I/II	乳癌	Moulder SL[9]
erlotinib	トラスツズマブ	II	乳癌 (first line)	UCLA-010620
erlotinib	bevacizumab	I/II	非小細胞肺癌	Sandler AB[10]
		I	大腸癌	JHOC-JO220
		I	頭頸部癌	Mauer AM[12]
		II	腎細胞癌	Hainsworth JD[13]
		II	乳癌	Dickler M[14]
トラスツズマブ	bevacizumab	I/II	乳癌	UCLA-0109030-03
トラスツズマブ	イマチニブ	I	固形癌	FCCC-03041
erlotinib+cetuximab	±bevacizumab	I/II	腎・大腸・頭頸・非小細胞肺癌	CTRC-IDD-0332

(筆者作成)

に相当するものとして，NSCLC に対する erlotinib と bevacizumab の併用などがあげられる．

分子標的治療薬併用の臨床試験

erlotinib＋bevacizumab[10]

Erlotinib はゲフィチニブと同じ EGFR-TKI で，EGFR の自己リン酸化部位への ATP 結合を競合的に阻害し，下流へのシグナル伝達を阻害する．一方，bevacizumab は血管内皮増殖因子（VEGF）を抗原として認識するヒト化マウス抗体であり，癌組織への栄養血管新生を抑制する（図❷）．

また，ヒト異種移植片において erlotinib と bevacizumab との併用は基礎レベルでの相乗効果が認められている[10)~12)]（図❸）．これらの背景をもとに米国において多施設共同で両剤併用の第 I/II 相試験がおこなわれた．対象は 1 レジメン以上の先行治療を有する IIIB もしくはIV期の NSCLC 患者 40 症例が登録された．投与方法は，erlotinib (100 もしくは 150 mg) 1 日 1 回連日 21 日間連続内服し，bevacizumab (7.5 もしくは 15 mg/kg) day 1 静注を 21 日ごとにくり返した．第 I 相部分の結果より推奨用量は erlotinib 150 mg，bevacizumab 15 mg/kg と設定され第II相部分に移行した．効果は PR 20%，SD 65%，PD 15%で，第II相部分での無増悪生存期

間中央値は6.2ヵ月，全生存期間中央値は12.6ヵ月と，それぞれの単剤での臨床試験よりも良好な結果が示された．毒性は皮疹，下痢，悪心が主であり，いずれも軽度から中等度であった．また2剤間の薬物相互作用は認めなかった．以上よりこれら2剤併用療法が有望であると結論されているが，この試験の登録症例には腺癌が多く，脳転移が除外されているため，もともと予後のよい症例群であった可能性もある．現在，頭頸部癌[12]，腎癌[13]，乳癌[14]で同様の第Ⅰ/Ⅱ相試験が進行中である．

おわりに―今後の展望―

従来の抗癌剤は非特異的に殺細胞効果をもたらしていたのに対し，分子標的治療薬は癌の増殖や進展にかかわる分子に特異的に作用することで抗腫瘍効果をもたらしている．分子標的治療薬を併用することは，癌細胞特異的に多方面からアプローチするため，より少ない毒性で抗腫瘍効果を高める可能性のある大変合理的な考え方である．

併用療法で複数のシグナル伝達経路を阻害することにより，耐性化を防ぎ，相乗効果をもたらすことが期待されており，いくつかの組み合わせについては，細胞株を用いた研究でそれが実証されている[11)15)]．今後は，基礎研究で有望とされる併用療法について，臨床研究で有効性を検証していく必要がある．大規模臨床試験で評価できる治療法は限られているため，真のベネフィットが期待できる治療法を第Ⅰ/Ⅱ相試験で適切に選別することも重要である．

また今後，分子標的治療薬の臨床応用に際しては，腫瘍に発現する標的分子の発現やゲノム情報の解析にもとづく個別化治療の重要性がますます高まると予想される．癌細胞の生物学的特性や各分子標的治療薬の作用機序にもとづいて適切な併用療法が確立し，低リスク高ベネフィットの治療法が一日でも早く臨床応用されることを期待したい．

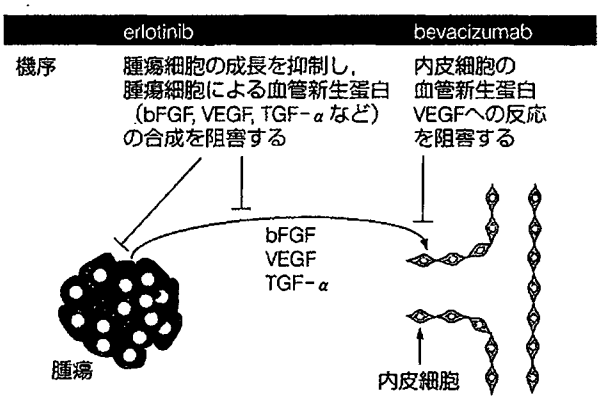

図❷ erlotinib と bevacizumab の併用の理論的背景
(Sandler AB *et al*, 2004[10]より改変引用)

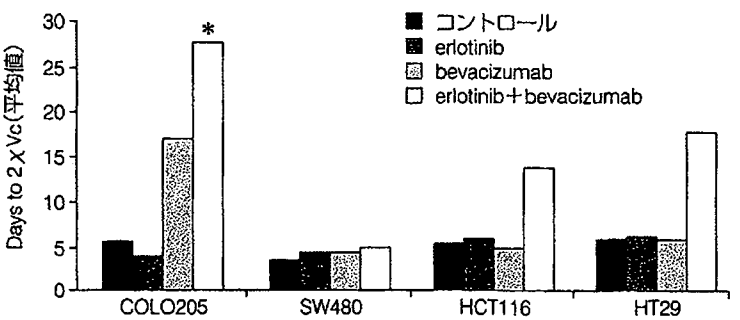

＊＞28 days to 2 X Vc
Genentech 社 Dr. M. Romero よりデータ提供

図❸ erlotinib と bevacizumab の相乗効果
(Sandler AB *et al*, 2004[10]より改変引用)

文献

1) Fukuoka M *et al*：Multi-institutional randomized phase II trial of gefitinib for previously treated patients with advanced non-small-cell lung cancer. *J Clin Oncol* **21**：2237-2246, 2003
2) Paez JG *et al*：EGFR mutations in lung cancer：correlation with clinical response to gefitinib therapy. *Science* **304**：1497-1500, 2004
3) Lynch TJ *et al*：Activation mutations in the epidermal growth factor receptor underlying

responsiveness of non-small-cell lung cancer to gefitinib. *N Engl J Med* **350**：2129-2139, 2004
4) Giaccone G *et al*：Gefitinib in combination with gemcitabine and cisplatin in advanced non-small-cell lung cancer：a phase III trial-INTACT 1. *J Clin Oncol* **22**：777-784, 2004
5) Herbst RS *et al*：Gefitinib in combination with paclitaxel and carboplatin in advanced non-small-cell lung cancer：a phase III trial-INTACT 2. *J Clin Oncol* **22**：785-794, 2004
6) Baselga J *et al*：Combining the anti-EGFR agent gefitinib with chemotherapy in non-small-cell lung cancer：how do we go from INTACT to impact? *J Clin Oncol* **22**：759-761, 2004
7) Baselga J：Targeting the epidermal growth factor receptor：a clinical reality. *J Clin Oncol* **19**：41 S-44 S, 2001
8) Normanno N *et al*：Cooperating inhibitory effect of ZD 1839 (Iressa) in combination with trastuzumab (Heceptin) on human breast cancer cell growth. *Ann Oncol* **13**：65-72, 2002
9) Moulder SL *et al*：A Phase I/II Trial of trastuzumab and gefitinib in patients with Metastatic Breast Cancer that overexpresses HER 2/neu (ErbB-2). *Clin Breast Cancer* **4**：142-145, 2003
10) Sandler AB *et al*：Phase I/II trial evaluating the anti-VEGF Mab bevacizumab in combination with erlotinib, a HER 1/EGFR-TK inhibitor, for patients with recurrent non-small cell lung cancer. (abstract No. 2000) *ASCO*：2004
11) Jung YD *et al*：Effects of combination anti-vascular endothelial growth factor receptor and anti-epidermal growth factor receptor therapies on the growth of gastric cancer in a nude mouse model. *Eur J Cancer* **38**：1133-1140, 2002
12) Mauer AM *et al*：Phase I study of epidermal growth factor receptor (EGFR) inhibitor, erlotinib, and vascular endothelial growth factor monoclonal antibody, bevacizumab, in recurrent and/or metastatic squamous cell carcinoma of the head and neck (SCCHN). (abstract No. 5539) *ASCO*：2004
13) Hainsworth JD *et al*：Phase II trial of bevacizumab and erlotinib in patients with metastatic renal carcinoma (RCC). (abstract No. 4502) *ASCO*：2004
14) Dickler M, *et al*：Phase II trial of erlotinib (OSI-774), an epidermal growth factor receptor (EGFR)-tyrosine kinase inhibitor, and bevacizumab, a recombinant humanized monoclonal antibody to vascular endothelial growth factor (VEGF), in patients with metastatic breast cancer. (abstract No. 2001) *ASCO*：2004
15) Ciardiello F *et al*：Epidermal growth factor receptor (EGFR) as a target in cancer therapy：understanding the role of receptor expression and other molecular determinants that could influence the response to anti-EGFR drugs. *Eur J Cancer* **39**：1348-1354, 2003

Enhancement of Sensitivity to Tumor Necrosis Factor α in Non–Small Cell Lung Cancer Cells with Acquired Resistance to Gefitinib

Koichi Ando,[1] Tohru Ohmori,[1,2] Fumiko Inoue,[2] Tsuyoki Kadofuku,[2] Takamichi Hosaka,[1] Hiroo Ishida,[1] Takao Shirai,[1] Kentaro Okuda,[1] Takashi Hirose,[1] Naoya Horichi,[1] Kazuto Nishio,[3] Nagahiro Saijo,[3] Mitsuru Adachi,[3] and Toshio Kuroki[4]

Abstract Tumor cells that have acquired resistance to gefitinib through continuous drug administration may complicate future treatment. To investigate the mechanisms of acquired resistance, we established PC-9/ZD2001, a non-small-cell lung cancer cell line resistant to gefitinib, by continuous exposure of the parental cell line PC-9 to gefitinib. After 6 months of culture in gefitinib-free conditions, PC-9/ZD2001 cells reacquired sensitivity to gefitinib and were established as a revertant cell line, PC-9/ZD2001R. PC-9/ZD2001 cells showed collateral sensitivity to several anticancer drugs (vinorelbine, paclitaxel, camptothecin, and 5-fluorouracil) and to tumor necrosis factor α (TNF-α). Compared with PC-9 cells, PC-9/ZD2001 cells were 67-fold more sensitive to TNF-α and PC-9/ZD2001R cells were 1.3-fold more sensitive. Therefore, collateral sensitivity to TNF-α was correlated with gefitinib resistance. PC-9/ZD2001 cells expressed a lower level of epidermal growth factor receptor (EGFR) than did PC-9 cells; this down-regulation was partially reversed in PC-9/ZD2001R cells. TNF-α-induced autophosphorylation of EGFR (cross-talk signaling) was detected in all three cell lines. However, TNF-α-induced Akt phosphorylation and IκB degradation were observed much less often in PC-9/ZD2001 cells than in PC-9 cells or PC-9/ZD2001R cells. Expression of the inhibitor of apoptosis proteins c-IAP1 and c-IAP2 was induced by TNF-α in PC-9 and PC-9/ZD2001R cells but not in PC-9/ZD2001 cells. This weak effect of EGFR on Akt pathway might contribute to the TNF-α sensitivity of PC-9/ZD2001 cells. These results suggest that therapy with TNF-α would be effective in some cases of non-small-cell lung cancer that have acquired resistance to gefitinib.

Gefitinib (Iressa, ZD1839), a small-molecule epidermal growth factor receptor (EGFR) tyrosine kinase inhibitor, has been approved for the treatment of refractory and relapsed non-small-cell lung cancer (NSCLC) patients in a number of countries around the world. This drug, which is given continuously as a once-daily oral dose, showed antitumor activity in patients with relapsed or recurrent NSCLC; however, tumor responses were observed in 12% to 18% of patients with chemotherapy-refractory advanced NSCLC (1, 2). Even in cases sensitive to gefitinib, resistance might be acquired through continuous drug administration. Additional treatments for cases of NSCLC relapsing during treatment with gefitinib are urgently needed.

To investigate the mechanism of acquired resistance to gefitinib, we previously established gefitinib-acquired resistant cells, PC-9/ZD2001, from a NSCLC, PC-9, which is hypersensitive to gefitinib and has a 15-del mutation in exon 19 of EGFR (data not shown). After >6 months of culture in gefitinib-free conditions, the sensitivity of PC-9/ZD2001 cells to gefitinib was restored, and the cells were subsequently established as a revertant cell line, PC-9/ZD2001R. The active mutation of EGFR was sustained in both the resistant and the revertant cell lines and the existence of revertant cell line suggests the additional mutation of EGFR, such as a secondary mutation of T790M in EGFR that causes resistance to gefitinib (3, 4), is unlikely to be contribute to this gefitinib resistance. In the gefitinib-resistant cells, the expression levels of EGFR and mRNA decreased to 30% to 50% of those in parental cells. A ligand-induced EGFR activation minimally activated mitogen-activated protein kinase signaling pathways and the inhibitory effect of gefitinib on this

Authors' Affiliations: [1]First Department of Internal Medicine and [2]Institute of Molecular Oncology, Showa University, Tokyo, Japan; [3]Internal Medicine, Pharmacology Division, National Cancer Center Hospital, National Cancer Center Research Institute, Tokyo, Japan; and [4]Gifu University, Gifu, Japan

Received 4/12/05; revised 8/10/05; accepted 8/26/05.

Grant support: Grant-in-Aid for a High-Technology Research Center Project from the Ministry of Education, Science, Sports, and Culture of Japan; Showa University Grant-in-Aid for Innovative Collaborative Research Projects; and Special Research Grant-in-Aid for Development of Characteristic Education from the Ministry of Education, Culture, Sports, Science, and Technology of Japan.

The costs of publication of this article were defrayed in part by the payment of page charges. This article must therefore be hereby marked *advertisement* in accordance with 18 U.S.C. Section 1734 solely to indicate this fact.

Requests for reprints: Tohru Ohmori, Institute of Molecular Oncology, Showa University, Hatanodai, 1-5-8, Shinagawa-ku, Tokyo 142-8555, Japan. Fax: 81-3-3784-2299; E-mail: ohmorit@med.showa-u.ac.jp.

doi:10.1158/1078-0432.CCR-05-0811

pathway was significantly decreased in the resistant cells.[5] To elucidate the cross-resistance to other anticancer agents, we examined the sensitivity to the conventional anticancer agents and tumor necrosis factor α (TNF-α). PC-9/ZD2001 showed cross-resistance to another EGFR inhibitor, AG1478. Interestingly, gefitinib-resistant cells were ~3-fold more sensitive than PC-9 cells to the cytotoxic effects of vinorelbine, paclitaxel, camptothecin, 5-fluorouracil, and a cytokine, TNF-α.[5] The same tendency was confirmed in the other gefitinib-resistant clones established along with PC-9/ZD2001. The restoration of these collateral sensitivities (except 5-fluorouracil) in revertant PC-9/ZD2001R cells suggests that such sensitivities are correlated with the mechanism of gefitinib resistance.

TNF-α is the prototype of ~20 related cytokines that act through specific members of the TNF receptor (TNFR) super family (5–7). Several cancer therapies exploiting the cytotoxic effect of TNF-α on solid tumors and soft-tissue sarcomas have recently been examined in clinical trials (8, 9). The TNF-α stimulates inflammation by turning on gene transcription through signaling cascades such as the Akt/nuclear factor κB (NF-κB) pathway. This signaling subsequently serves as the primary mechanism to protect cells against apoptotic stimuli through several transcriptional genes, such as inhibitor of apoptosis proteins (IAP), the specific inhibitor of caspases (10, 11). In contrast, TNF-α-mediated signaling also triggers apoptosis through the activation of caspase-8 and the downstream caspase-3 or caspase-7 in a wide variety of cells (12). From these observations, it is possible to say that TNF-α has two different signaling pathways that contradict each other. The cytotoxic effect of TNF-α might be determined by ratios between the apoptosis-inducing and the apoptosis-inhibiting effects.

Akt/NF-κB signaling also occurs downstream of EGFR and this signaling mediates cell proliferation and antiapoptotic signaling through this pathway (13). In the case of the antiapoptotic signaling of TNF-α, TNFR is known to activate Akt/NF-κB in three ways: directly through phosphatidylinositol 3-kinase activation, or indirectly through cross-talk signaling to EGFR, or both together (5–7, 12, 14, 15). Moreover, several recent articles report that the TNFR-mediated cross-talk signaling to EGFR occurs in a ligand-dependent and -independent manner (16–21). Therefore, to investigate the mechanisms of the collateral sensitivity to TNF-α in gefitinib-acquired resistant cells, we focused on TNF-α-induced cross-talk signaling to EGFR and analyzed the Akt/NF-κB signaling pathway in response to TNF-α.

In this article, we show that a weakness of Akt/NF-κB signaling from TNF-α-mediated cross-talk signaling via EGFR causes the collateral sensitivity to TNF-α in the gefitinib-acquired resistant cell line. Moreover, this cross-talk signaling is thought to be a dominant pathway of TNF-α-mediated Akt activation.

Materials and Methods

Chemicals and antibodies. Gefitinib was donated by AstraZeneca Pharmaceuticals (Wilmington, DE). An anti-phospho-EGFR antibody (Tyr1068) was purchased from Cell Signaling Technology (Beverly, MA). Other antibodies and chemicals were purchased from Santa Cruz Biotechnology, Inc. (Santa Cruz, CA) and Sigma-Aldrich Co. (St. Louis, MO), respectively, unless otherwise specified.

Cell lines and cultures. The PC-9 human NSCLC cell line, established from a previously untreated patient, was kindly donated by Prof. K. Hayata (Tokyo Medical College, Tokyo, Japan.). The PC-9 cells were cultured with RPMI 1640 supplemented with 10% FCS and maintained in a 5% CO_2 incubator at 37°C under humidified conditions.

Establishment of gefitinib-resistant cell lines. To establish gefitinib-resistant cell lines, PC-9 cells were continuously exposed to increasing dosages of gefitinib for >1 year. The surviving cells were cloned and three gefitinib-resistant cell lines, designated as PC-9/ZD2001, PC-9/ZD2002, and PC-9/ZD2003, were established. These cell lines can survive exposure to 200 nmol/L gefitinib. Sensitivity to gefitinib was restored by culture of PC-9/ZD2001 in gefitinib-free conditions for >6 months. The restored cells were cloned and subsequently established as a revertant cell line, PC-9/ZD2001R.

Established resistant cell lines were maintained by culture in a medium containing 200 nmol/L gefitinib. To eliminate the effects of gefitinib, the resistant cells were cultured in a drug-free medium for at least 2 weeks before all experiments. As the relative resistance values of these cell lines were stable for at least 3 months after culture under drug-free conditions (data not shown), we used the cells for experiments during this period.

Growth inhibition assay. To measure sensitivity to gefitinib, a 3-(4,5-dimethylthiazol-2-yl)-2,5-diphenyltetrazolium bromide assay was done (Cell Titer 96 assay kit, Promega Corp., Madison, WI). In brief, PC-9, PC-9/ZD2001, and PC-9/ZD2001R cells were seeded onto 96-well plates and preincubated overnight. The cells were continuously exposed to the indicated concentrations of gefitinib for 4 or 5 days. Absorbance was measured at 570 nm with a microplate reader (Model 550, Bio-Rad Laboratories, Hercules, CA).

Analysis of tumor necrosis factor α–induced apoptotic cell death. The PC-9, PC-9/ZD2001, and PC-9/ZD2001R cells were treated with 100 ng/mL TNF-α for the indicated time periods. They were then fixed with 4% paraformaldehyde at 4°C for 30 minutes. After 100 μL of 70% ethanol were added, the cells were permeabilized by incubation overnight at −20°C. Apoptotic DNA fragments were probed with the terminal deoxyribonucleotidyl transferase-mediated dUTP nick end labeling method (MEBSTAIN Apoptosis TUNEL Kit Direct, Medical & Biological Laboratories, Nagoya, Japan) and subpopulations of apoptotic cells were measured with a flow cytometer (FACSCalibur, BD Biosciences Immunocytometry Systems, San Jose, CA).

Activity assays for CPP32/caspase-3 and FLICE/caspase-8. Activities of CPP32/caspase-3 and FLICE/caspase-8 were measured with caspase-3 and caspase-8 colorimetric assay kits (MRL Diagnostics, Cypress, CA) according to the instructions of the manufacturer. The PC-9, PC-9/ZD2001, and PC-9/ZD2001R cells were incubated for 12 hours with 10 ng/mL TNF-α and then resuspended in 50 μL of chilled cell lyses buffer. The cells were incubated on ice for 10 minutes and the protein concentration of the supernatant was assayed with a bicinchoninic acid protein assay kit (Sigma-Aldrich). A certain amount of each sample was added to 50 μL of 2× reaction buffer containing the respective substrates DEVD-pNA and IETD-pNA, then incubated at 37°C for 1 hour. After incubation, absorbance was measured at 400 and 405 nm with a microtiter plate reader (Model 550, Bio-Rad Laboratories).

Immunoblot analysis. Cells were treated with 10 ng/mL of TNF-α for 30 minutes, then washed twice with ice-cold PBS and lysed in EBC buffer [50 mmol/L Tris-HCl (pH 8.0), 120 mmol/L NaCl, 0.5% NP40, 100 μmol/L NaF, 200 μmol/L Na orthovanadate, and 10 μg/mL of leupeptin, aprotinin, and phenylmethylsulfonyl fluoride] with an ultrasonic disrupter (Tomy Digital Biology Co., Ltd., Tokyo, Japan). The cell lysate was precleared by centrifugation, resolved by 10% SDS-PAGE, transferred to nitrocellulose membrane, and probed with antibodies against EGFR, phospho-EGFR (Tyr1045), phosphatase and tensin homologue, Akt, phospho-Akt, IκB, c-IAP1, and c-IAP2. Bound antibodies were detected with horseradish peroxidase-linked immunoglobulin (Amersham Biosciences, Buckinghamshire, United Kingdom)

[5] T. Yamaoka, T. Ohmori, F. Inoue, et al. Characteristics of gefitinib-acquired resistance in non–small cell lung cancer cell lines, submitted for publication.

and enhanced chemiluminescence reagents (Perkin-Elmer Life and Analytical Sciences, Boston, MA).

Real-time reverse transcription-PCR method. Total RNA was isolated with the guanidium isothiocyanate method using an RNA purification kit (RNeasy Mini Kit, Qiagen, Venlo, the Netherlands) according to the instructions of the manufacturer. After RNA isolation, cDNA was prepared in the presence of random 9-mers with a reverse transcription-PCR (RT-PCR) kit (Takara Shuzo Co., Ltd., Kyoto, Japan). Expression levels of EGFR, c-IAP1, and c-IAP2 mRNA were quantified with a fluorescence-based real-time detection method (GeneAmp 5700 Sequence Detection System, Applied Biosystems, Foster City, CA). Cycling conditions were 40 cycles at 94°C for 20 seconds, 55°C (EGFR) and 64°C (c-IAPs) for 20 seconds, and 72°C for 30 seconds. Expression of the mRNA was measured with the following primer sets: EGFR, 5′-ACGAATGGGCCTAAGATC-3′ and 5′-TGCTTACCCGGATTCTAGG-3′; c-IAP1, 5′-ATGTGGGTAACAGTGATGATGTCA-3′ and 5-AAACCAC-TTGGCATGTTGAAC-3′; and c-IAP2, 5′-CTAGTGTTCATGTTGAAC-3′ and 5′-CCTCAAGCCACCATCACAAC-3′. The expression of β-actin mRNA was used as an internal control.

Statistical analysis. Statistical analysis was done with the StatView II software program (Abacus Concepts, Berkeley, CA). Activities of CPP32/caspase-3 and FLICE/caspase-8 were analyzed with paired Student's t test. $P < 0.05$ was considered significant.

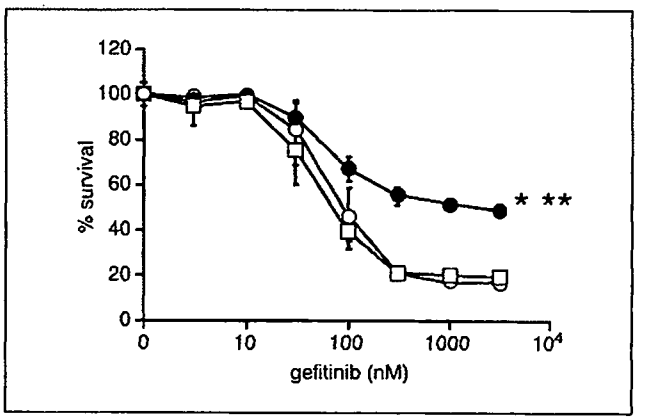

Fig. 1. Cytotoxic effects of gefitinib in a gefitinib-resistant NSCLC cell line. The cells (2×10^3 per well) were seeded onto a 96-well plate and preincubated overnight, then continuously exposed to the indicated concentrations of gefitinib for 4 or 5 days. The growth inhibition rate was analyzed with 3-(4,5-dimethylthiazol-2-yl)-2,5-diphenyltetrazolium bromide assay as described in Materials and Methods. ○, PC-9; ●, PC-9/ZD2001; □, PC-9/ZD2001R. Points, mean of three different experiments; bars, SD. *, $P < 0.001$, PC-9 versus PC-9/ZD2001; **, $P < 0.001$, PC-9/ZD2001R versus PC-9/ZD2001.

Results

Establishment of acquired gefitinib-resistant cell lines. To elucidate the mechanism of acquired resistance against gefitinib, we established gefitinib-resistant NSCLC cell lines through continuous exposure of this drug. Resistance against gefitinib developed quite slowly; the relative resistant values of 3- to 4-fold were reached after >1-year exposure to gefitinib. We picked the clones of gefitinib-resistant cell lines named PC-9/ZD2001, PC-9/ZD2002, and PC-9/ZD2003. These cell lines can survive in 200 nmol/L gefitinib-contained medium. Sensitivities to gefitinib were measured by 3-(4,5-dimethylthiazol-2-yl)-2,5-diphenyltetrazolium bromide assay. In the case of PC-9/ZD2001 cells, the cell line was able to survive by >50% at the concentration of >500 nmol/L gefitinib. This concentration caused maximum inhibition in PC-9. The IC_{40} value of gefitinib in PC-9 cells was 53.0 ± 8.1 nmol/L. The gefitinib-resistant cell line PC-9/ZD2001 showed a 4-fold higher resistance to gefitinib than PC-9 cells (IC_{40} = 211.1 ± 32.4 nmol/L; Fig. 1). Culture of the cells in gefitinib-free conditions for 6 months restored sensitivity to gefitinib in PC-9/ZD2001 and subsequently established a revertant cell line, PC-9/ZD2001R, in which sensitivity to gefitinib was completely restored (IC_{40} = 46.3 ± 10.2 nmol/L).

Analysis for tumor necrosis factor α–induced apoptotic cell death. TNF-α-induced cytotoxic effect was measured by 3-(4,5-dimethylthiazol-2-yl)-2,5-diphenyltetrazolium bromide assay. The IC_{40} values of TNF-α in PC-9, PC-9/ZD2001, and PC-9/ZD2001R cell lines were 815.0 ± 44.8, 12.2 ± 1.4, and 626.2 ± 18.5 ng/mL, respectively. PC-9/ZD2001 cells acquired new sensitivity to TNF-α. PC-9/ZD2001 was ~67-fold more sensitive to TNF-α as compared with PC-9, but this sensitization was restored to 1.3-fold in PC-9/ZD2001R (Fig. 2A). This collateral sensitivity to TNF-α was confirmed in the other gefitinib-resistant cell lines, PC-9/ZD2002 and PC-9/ZD2003 (data not shown).

Additionally, we measured TNF-α-induced apoptotic cell death by flow cytometry. The apoptotic cells were stained by the terminal deoxyribonucleotidyl transferase-mediated dUTP nick end labeling method. No significant apoptosis was observed in these three cell lines until 24 hours of exposure to TNF-α (10 ng/mL). Forty-eight hours of TNF-α exposure induced a 6-fold higher apoptotic cell death in PC-9/ZD2001 cells (70.3%) as compared with the parental PC-9 cells (11.8%). This enhancement was completely recovered in PC-9/ZD2001R cells (16.6%; Fig. 2B; Table 1). These results suggest that the collateral sensitivity to TNF-α might be correlated with the resistance to gefitinib in these cell lines.

Analysis of tumor necrosis factor α–mediated activations of CPP/caspase-3 and FLICE/caspase-8. To clarify the difference of TNF-α-induced apoptotic cell death in these cell lines, we analyzed TNF-α-mediated CPP32/caspase-3 and its upstream FLICE/caspase-8 activations by caspase-8 and caspase-3 colorimetric protease assay kits (Medical and Biological Laboratories), respectively. PC-9, PC-9/ZD2001, and its revertant PC-9/ZD2001R cells were incubated with the indicated concentrations of TNF-α for 12 hours. In the case of caspase-3, TNF-α did not cause any increases in the activity in PC-9 and PC-9/ZD2001R cells even at the highest concentration of 100 ng/mL. In contrast, TNF-α significantly enhanced caspase-3 activity in PC-9/ZD2001 cells even at the concentration of 1 ng/mL within this time course (Fig. 3A). In the case of caspase-8, TNF-α enhanced the activities in all three cell lines from 10 ng/mL (Fig. 3B). TNF-α at 100 ng/mL activated caspase-8 ~1.6-, 2.9-, and 1.9-fold higher in PC-9, PC-9/ZD2001, and PC-9/ZD2001R, as compared with the respective untreated cells. In PC-9/ZD2001 cells, TNF-α caused the highest relative induction of caspase-8 (Fig. 3B).

Immunoblot analysis for the tumor necrosis factor α–induced cross-talk signaling to epidermal growth factor receptor and Akt/nuclear factor κB pathway activation. EGFR expression was significantly lower in PC-9/ZD2001 than in PC-9 cells (Fig. 4A). When measuring the expression of EGFR protein by a densitometer (calculated by the NIH image software), the expression was decreased to 52.4 ± 2.6% of that in parental cell line. Moreover, we measured the expression levels of EGFR mRNA by a real-time RT-PCR method. The expression level in PC-9/ZD2001 was decreased to 37.0 ± 3.2% of that in parental

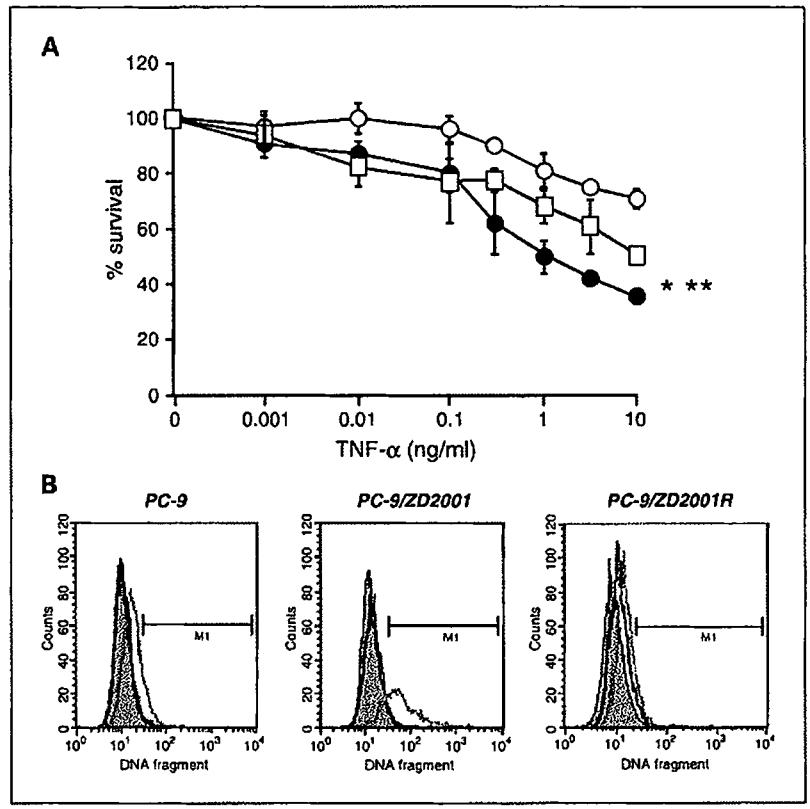

Fig. 2. Gefitinib-resistant cells acquired sensitivity to TNF-α. *A*, the cells were continuously treated with the indicated concentrations of TNF-α for 4 or 5 days. The growth inhibition rate was analyzed with 3-(4,5-dimethylthiazol-2-yl) -2,5-diphenyltetrazolium bromide assay as described in Materials and Methods. ○, PC-9; ●, PC-9/ZD2001; □, PC-9/ZD2001R. PC-9/ZD2001 cells were ~67-fold more sensitive to TNF-α than were PC-9 cells but the sensitivity of revertant PC-9/ZD2001R cells decreased to 1.3-fold that in PC-9 cells. Points, mean of three different experiments; bars, SD. *, $P < 0.001$, PC-9 versus PC-9/ZD2001, **, $P < 0.001$, PC-9/ZD2001R versus PC-9/ZD2001. *B*, the cells were treated with 10 ng/mL TNF-α for the indicated time periods. After treatment, the cells were fixed with 4% paraformaldehyde at 4°C and permeabilized with 70% ethanol. Fragments of apoptotic DNA were stained with the terminal deoxyribonucleotidyl transferase-mediated dUTP nick end labeling method and measured with flow cytometry as described in Materials and Methods.

cells. The same down-regulation of EGFR was seen in the other resistant cell lines (data not shown). In the case of PC-9/ZD2001R, expression levels of EGFR protein and mRNA were also decreased to 69.3 ± 1.1% and 56.8 ± 2.2%, respectively, as compared with PC-9. The expression of EGFR was restored, but not completely, in the revertant cell line.

In PC-9 cells, cross-talk signaling from TNFR to EGFR was observed and treatment with 10 ng/mL TNF-α for 30 minutes induced significant autophosphorylation of EGFR (Fig. 4A). According to the autophosphorylation of EGFR, definite phosphorylation of Akt and a decrease in IκB content were observed. The activation of Akt and down-regulation of IκB were inhibited by gefitinib at concentrations <10 nmol/L. Because gefitinib (100 nmol/L) mostly inhibited this signaling, we concluded that the cross-talk signaling from TNFR to EGFR might be the dominant pathway of TNF-α-mediated Akt/NF-κB activation in this cell line rather than the direct signaling from TNFR to Akt. In contrast, although EGFR autophosphorylation was observed, only partial phosphorylation of Akt and down-regulation of IκB, compared with those in PC-9, were observed after TNF-α exposure in PC-9/ZD2001 cells (Fig. 4A and B). Treatment with gefitinib inhibited this cross-talk signaling to EGFR but had no effect on downstream Akt phosphorylation.

These observations suggest that TNF-α-mediated EGFR signaling has less effect on the Akt/NF-κB pathway in the gefitinib-resistant PC-9/ZD2001 cell line. Other stimuli might activate Akt in an EGFR-independent manner. In the revertant PC-9/ZD2001R cell line, this weak effect of EGFR was largely reversed and TNF-α exposure induced autophosphorylation of EGFR and subsequent activation of the Akt/NF-κB pathway. The expression levels of phosphatase and tensin homologue, a suppressor of Akt signaling, did not differ significantly among PC-9, PC-9/ZD2001, and PC-9/ZD2001R cells. This decreased effect of EGFR might be partially caused by the down-regulation of EGFR expression in PC-9/ZD2001. However, although the EGFR-mediated signaling and the resistance to gefitinib were mostly restored, EGFR expression remained only partially restored in PC-9/ZD2001R. For this reason, we speculated that the down-regulation of EGFR expression might not fully explain the weak EGFR signaling to Akt pathway in PC-9/ZD2001 cells.

To clarify the decreased EGFR signaling in PC-9/ZD2001, we examined the inhibitory effect of a phosphatidylinositol 3-kinase inhibitor, wortmannin, on the TNF-α-induced activation of this pathway (Fig. 4B). Interestingly, wortmannin inhibited the TNF-α-mediated phosphorylation of Akt in PC-9/ZD2001 cells at the same level as it did in PC-9 and PC-9/ZD2001R cells.

Expresstion of c-IAP1 and c-IAP2 on treatment with tumor necrosis factor α. After treatment with TNF-α (10 ng/mL) for 30 minutes, expression of c-IAP1 and c-IAP2 proteins was

Table 1. Percentage of apoptotic subpopulations

%Apoptosis	PC-9	PC-9/2001	PC-9/2001R
Control	1.1	1.2	1.1
24 h	1.4	2.3	3.2
48 h	11.8	70.3	6.6

NOTE: After 72 hours of exposure to TNF-α, significant apoptotic cell death was observed in PC-9/ZD2001 cells but not in PC-9 or PC-9/ZD2001R cells.

significantly increased in PC-9 and PC-9/ZD2001R cells but not in PC-9/ZD2001 cells (Fig. 4A and B). According to the results of Akt phosphorylation, induction was inhibited by gefitinib in PC-9 and PC-9/ZD2001R cells but not in PC-9/ZD2001 cells. Wortmannin could inhibit induction in all three cell lines. Consistent with the results of protein expression, treatment with TNF-α increased the expression level of c-IAP1 and c-IAP2 mRNA in PC-9 and PC-9/ZD2001R cells in a dose-dependent manner (Fig. 5A and B). After treatment with 100 ng/mL TNF-α for 12 hours, the expression levels of both c-IAP1 and c-IAP2 mRNA were significantly increased in PC-9 cells (c-IAP1, 7.05 ± 0.62; c-IAP2, 18.22 ± 0.25) and PC-9/ZD2001R cells (c-IAP1, 7.02 ± 0.54; c-IAP2, 11.56 ± 0.75) but not in PC-9/ZD2001 cells (c-IAP1, 2.60 ± 0.58; c-IAP2, 2.83 ± 0.66). These observations suggest that TNF-α-induced apoptotic signaling is not inhibited by its own antiapoptotic effects, such as IAPs induction, owing to the weak effect of TNF-α-mediated signaling and the Akt/NF-κB pathway via EGFR in this gefitinib-resistant cell line.

Discussion

We have shown that the gefitinib-acquired resistant NSCLC cell line PC-9/ZD2001 acquired collateral sensitivity to the apoptotic effect of TNF-α. Because this collateral sensitivity was significantly diminished in the revertant PC-9/ZD2001R, it might be correlated with gefitinib resistance. As described before, PC-9/ZD2001 also acquired collateral sensitivities to some anticancer drugs, such as vinorelbine, paclitaxel, camptothecin, and 5-fluorouracil. However, this cell line did not show the collateral sensitivities to cisplatin, etoposide, mitomycin C, and cyclophosphamide.[5] Moreover, there was no difference of susceptibility to serum-starved condition between PC-9 and PC-9/ZD2001 (data not shown). From these observations, it can be concluded that the collateral sensitivities of the gefitinib-resistant cells are specific to some cell stresses and are not caused by the fragility of the cells. Because the same tendency of sensitivity was seen in the other resistant clones, PC-9/ZD2002 and PC-9/ZD2003, the acquired sensitivity to the anticancer drugs and TNF-α could be a general phenomenon even in the clinical gefitinib-resistant cells.

TNF-α activates not only apoptotic signaling but also antiapoptotic signaling via the Akt/NF-κB activation (22, 23). Activation of the downstream transcription factor NF-κB inhibits various types of apoptotic cell death by inducing apoptotic inhibitory proteins (22, 23), such as bcl-2 (24), bcl-xl (25), forkhead (26), and IAPs (10, 11, 27, 28). As described before, it is thought that the cytotoxic effect of TNF-α is determined by ratios between the apoptosis-inducing and the apoptosis-inhibiting effects (5–7, 12, 14, 15).

In parental PC-9 cells, TNF-α induced EGFR autophosphorylation and subsequent Akt/NF-κB pathway activation (Fig. 4A and B). This autophosphorylation was completely inhibited by a low concentration of gefitinib (10 nmol/L). From these observations, we think that TNF-α-induced Akt/NF-κB pathway activation occurs mainly through cross-talk from TNFR to EGFR in this cell line. Because the expression level of EGFR was significantly decreased in PC-9/ZD2001 as compared with the parental PC-9, the decline of the cross-talk signaling might partially diminish the TNF-α-induced activation of the Akt/NF-κB pathway. Our results are supported by those of an earlier study showing that resistance to the cytotoxic effect of TNF-α is associated with high expression of Her family receptors, such as EGFR (Her1), erbB2/Her2/neu, or Her3, in a panel of human tumor cell lines (29). However, the decreased EGFR signaling from the Akt/NF-κB pathway could not be fully explained by the lower EGFR expression in PC-9/ZD2001 because EGFR expression remained only partially restored in the revertant PC-9/ZD2001R cell line. In light of these observations, to clarify the mechanisms of collateral sensitivity to TNF-α in the gefitinib-resistant cells, we focused on the cross-talk signaling from TNFR to EGFR in PC-9, PC-9/ZD2001, and PC-9/ZD2001R cells.

Several recent articles have reported that TNFR mediates cross-talk signaling to EGFR through a ligand-dependent and -independent manner (16–19, 21, 23). Chan et al. (17) have reported that exposure of human mammary epithelial cells to TNF-α results in transactivation of EGFR through metalloprotease-dependent shedding of EGFR ligand(s). Hirota et al. (18) reported that EGFR transactivation by TNF-α is

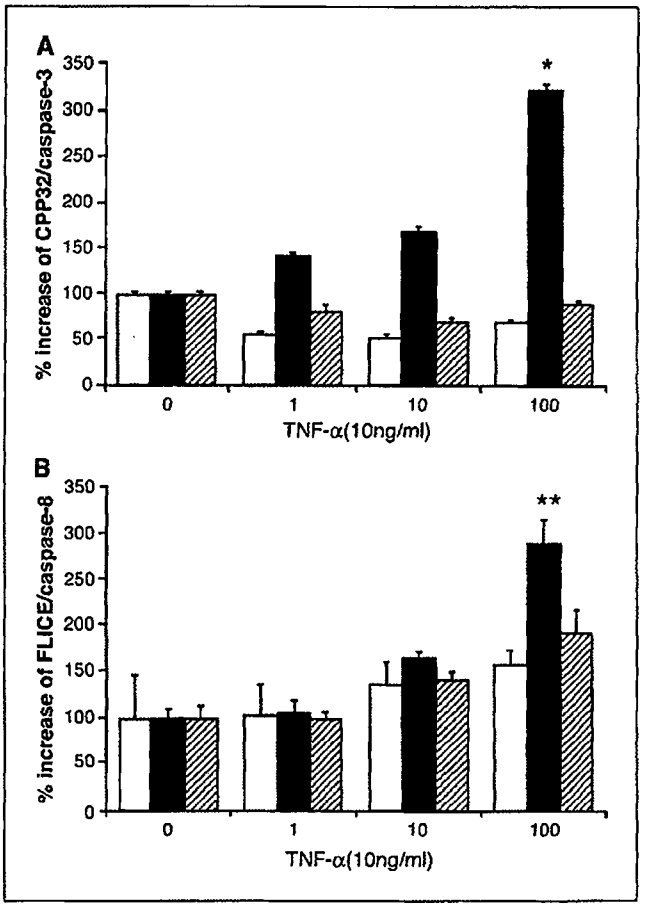

Fig. 3. TNF-α-mediated activation of CPP32/caspase-3 and FLICE/caspase-8 in PC-9, PC-9/ZD2001, and PC-9/ZD2001R cells. Activation of CPP32/caspase-3 and FLICE/caspase-8 was measured as described in Materials and Methods. The cells were exposed to the indicated concentrations of TNF-α for 12 hours; after which equivalent amounts of samples were reacted with the substrates DEVD-pNA and IETD-pNA. Absorbance was measured at 400 and 405 nm with a microtiter plate reader. *A*, CPP32/caspase-3. *B*, FLICE/caspase-8. TNF-α activated FLICE/caspase-8 in all three cell lines but activated CPP32/caspase-3 only in PC-9/ZD2001 cells. Data calculated as the percentage increase compared with respective untreated controls. Points, mean of three different experiments each done in triplicate; bars, SD. Open columns, PC-9; closed columns, PC-9/ZD2001; hatched columns, PC-9/ZD2001R. *, $P < 0.001$, PC-9 versus PC-9/ZD2001. **, $P = 0.02$, PC-9 versus PC-9/ZD2001.